

Chapter 7

Site Characterization

Auli Niemi, Katriona Edlmann, Jesus Carrera, Christopher Juhlin, Alexandru Tatomir, Iulia Ghergut, Martin Sauter, Jacob Bensabat, Fritjof Fagerlund, Francois H. Cornet, Victor Vilarrasa and Christopher Ian McDermott

Abstract A necessary first step in qualifying a specific site for CO₂ storage and for quantifying its relevant properties is a proper site characterization. Site characterization provides the ultimate input data for reservoir modeling and for all the predictions concerning the storage complex and its surroundings. It also provides baseline information for monitoring the behavior of injected CO₂. It also incorporates input from laboratory experiments described in Chap. 6. This chapter gives an overview of site characterization procedures with respect to geological storage of CO₂, by starting

A. Niemi (✉) · C. Juhlin · F. Fagerlund
Department of Earth Sciences, Uppsala University, Villavägen 16, Uppsala, Sweden
e-mail: Auli.Niemi@geo.uu.se

K. Edlmann · C.I. McDermott
School of Geoscience, Edinburgh Collaborative of Subsurface
Science and Engineering (ECOSSE), University of Edinburgh, Edinburgh, UK
e-mail: katriona.edlmann@ed.ac.uk

J. Carrera · V. Vilarrasa
Groundwater Hydrology Group (GHS UPC-CSIC), Institute of Environmental Assessment
and Water Research (IDAEA), Spanish National Research Council (CSIC),
Barcelona, Spain
e-mail: jesus.carrera.ramirez@gmail.com

V. Vilarrasa
e-mail: victor.vilarrasa@upc.edu

A. Tatomir · I. Ghergut · M. Sauter
Angewandte Geologie, Universität Göttingen, Goldschmidtstr. 3,
37077 Göttingen, Germany
e-mail: alexandru.tatomir@geo.uni-goettingen.de

J. Bensabat
Environmental and Water Resources Engineering Inc., P.O. Box 6770,
31067 Haifa, Israel
e-mail: jbensabat@ewre.com

F.H. Cornet
Institut de Physique du Globe–Strasbourg, Paris, France
e-mail: francois.cornet@unistra.fr

from regulatory requirements and guidelines and proceeding to specific methodologies for assessing the sites properties in terms of CO₂ geological storage.

7.1 Background

A necessary first step in qualifying a specific site for CO₂ storage and for quantifying its relevant properties, is a proper site characterization. Site characterization provides the input data for reservoir modeling and for all the predictions concerning the storage complex, as well as baseline information for monitoring the behavior of the injected CO₂. Site characterization models can be divided into static models, describing the existing geological conditions and fluid properties, and dynamic models where the dynamic behavior of fluid flow, stress field and the like are addressed by means of a dynamic reservoir simulations, by using the static model as the input data.

For site evaluation of the large scale structures, i.e. the caprock and the reservoir stratigraphy, their petrophysical and fluid properties must all be characterized. There is a range of relevant data sources that cover measurement scales from seismic data at the scale of kilometers to thin sections at the scale of microns, each capturing specific features and the heterogeneity of the reservoir. Site characterization methodologies are well known from a number of other geological and geo-engineering applications. In addition, geological storage of CO₂ poses some specific requirements in terms of site's suitability.

In the European perspective, detailed instructions on what should be addressed in a CO₂ storage project have been outlined in the EU directive for CCS (EU 2009). There, the procedure is divided in the steps of (i) data collection, (ii) building the 3-dimensional static model and (iii) characterization of the storage dynamic behavior, sensitivity characterization and risk assessment. In terms of data collection it is defined that sufficient data should be collected to construct a static model for the storage site, including the caprock, the surrounding area and the hydraulically connected areas. The data should cover at least geology and geophysics; hydrogeology; reservoir engineering; geochemistry; geomechanics; seismicity; presence and conditions of possible leakage pathways. The 3-dimensional geological model should characterize the storage complex in terms of the EU directive EU (2009) which includes: (a) geological structure of the physical trap; (b) geomechanical, geochemical and flow properties of the reservoir overburden (caprock seals, porous and permeable horizons) and surrounding formations; (c) fracture system characterization and presence of any human-made pathways; (d) areal and vertical extent of the storage complex; (e) pore space volume (including porosity distribution); (f) baseline fluid distribution; (g) other relevant characteristics. The third step, step for characterization of the storage dynamic behavior, sensitivity characterization and risk assessment is defined that it shall be based on dynamic modeling of CO₂ injection into the storage formation, using the above geological model. The directives also state what phenomena needs to be modeled. Dynamic modeling is discussed elsewhere in this book (Chap. 4 in particular). Here we will only exemplify the construction of the structural geological model as well

as give examples of data that is needed for the modeling. DNV (2010) has given guidelines for site selection and quantification of sites and projects for CO₂ storage, largely referring to the above EU directives. They also point out that the specific data required to address the requirements may depend on the site and that the developer should therefore be given discretion to select techniques necessary to be used to obtain the information and meet the objectives set.

In the US perspective, NETL (2013) in their recommendations for Best Practices for Site screening, Site selection and Initial Characterization for Storage of CO₂ in Deep Geologic Formations divide the steps of characterizing a potential CO₂ storage site as discussed below. The first ones of these steps are not actual site characterization but will nevertheless provide relevant information for site characterization, and are therefore included here.

According to NETL (2013) site screening is a stage where regional geological data is evaluated and analyzed in terms of (i) Injection formation: identifying regional and sub-regional formations that have suitable characteristics for storage; (ii) Adequate depth: it is ensured that formations have regional depth sufficient so that CO₂ remains in supercritical state; (iii) Confining zone; ensuring that there is adequate confining zone with sufficient lateral extent to avoid vertical migration of the CO₂ and (iv) Prospective storage resources: calculating the prospective storage resources to see that the reservoirs have sufficient pore volumes and can tolerate the pressure changes to accommodate the planned injection volumes. Table 7.1 summarizes in shortened form the NETL guidelines for Site Screening in terms of the regional geological data (excluding the regional and social aspects of site screening that are also discussed in the original report). Some of the issues identified are specific to the conditions in the US but can still be used as reference framework for other locations as well.

Next step, the site selection, is a stage to further evaluate the previously selected areas and develop a shorter list of sites that can be taken further to initial site characterization. The analyses related to geological data at this stage are summarized in Table 7.2. Initial characterization in turn is a stage after site selection stage. The subsurface data analysis is expanded to integrate the elements of the baseline data analysis, including geological, geochemical, geomechanical, hydrogeologic and flux data. Table 7.3 summarizes the issues to be addressed at this stage, in terms of the geoscientific data. Site Characterization then builds on the previous studies to develop a more detail characterization of the site. This could include additional drilling and testing of wells, to analyze geochemical and geomechanical properties, including stimulation testing to analyze injectivity, possible additional seismic surveys and brine injection tests to study the interference and pressure responses. At this stage continuity of the injection zones and confining zones needs to be established and potential leakage issues identified. NETL (2013) does not go into the details of this actual site characterization phase.

In the following sections we will describe some important site characterizations methods, in terms of geological storage of CO₂. We do not attempt to give a full account of all the site characterization techniques, partly as many of these methods are known from a number of different geoscientific and geoengineering applications. We also want to refer to a book specifically focusing on site characterization in the context of geological storage of CO₂ by Surdam (2013). The methods

Table 7.1 NETL guidelines for site screening in terms of geological factors (shortened from NETL 2013)

Element	Guidelines for site screening—geoscientific aspects
Injection formation	Identify formation types for potential injection. Utilize readily accessible data from public sources or from private firms. Data should include regional lithology maps, injection zone data (thickness, porosity, permeability), structural maps, information about structure closure and features that might compartmentalize the reservoir such as stratigraphic pinch outs, regional type logs, offset logs, petrophysical data, and regional seismicity maps
Adequate depth	Assessment of minimum depth of the injection zone to protect drinking water resources. In addition depths of at least 800 m generally indicate CO ₂ will be in a supercritical state and may be more cost-effectively stored. Shallow depths (<800 m) may add to the risk profile because CO ₂ could be in gas phase and the injection zone may be closer to drinking water sources
Confining system	Injection zones should be overlain by confining system comprised of one or more thick and impermeable zones of sufficient lateral extent. Confining systems can be identified from the same types of information used to identify injection formations. Wells that penetrate potential confining systems should be identified (sources e.g. oil and gas regulatory agencies). Faulting and folding information that may impact confinement integrity should be mapped along with potential communication pathways. Confining system integrity may be validated by presence of nearby hydrocarbon accumulations
Prospective storage resources	Candidate CO ₂ formations should contain enough prospective storage resources beneath a robust confining system. Prospective storage resources (and injectivity if permeability data is available) should be estimated at the sub-regional scale utilizing existing data (e.g. state geological surveys) to populate basic numerical models.

Table 7.2 NETL guidelines for site selection in terms of geoscientific aspects (shortened from NETL 2013)

Element	Guidelines for site selection—geoscientific aspects
Injection zone (reservoir)	Define injection zones based on public and acquired regional well data. Analysis should include at minimum the development of a regional stratigraphic column identifying potential storage types and injection and confining zone(s), potential USDWs (underground sources of drinking water); structure and isopach maps of injection and confining zone(s); regional cross-sections; regional tectonic maps, reservoir dip, and analog well data such as lithology, porosity, permeability, pressure, temperature, and dynamic formation evaluation data (DST, well test, production/injection data)
Confining system	Establish the areal extent, thickness, lithology, porosity, permeability, capillary pressure data, and other factors that might affect integrity of the confining system with confining zone(s). Perform a faulting and folding analysis based on tectonic history and analogs. Utilize existing well bore, core, outcrop and regional analog data to identify and map confining zone(s) tops, bases and thicknesses

(continued)

Table 7.2 (continued)

Element	Guidelines for site selection—geoscientific aspects
Trapping mechanisms	There are several mechanisms that effectively “trap” injected CO ₂ , including physical barriers, as well as physical and geochemical processes. Evaluation of trapping mechanism should be based on the local well, outcrop and any available regional reservoir analyses including analogs in similar formations
Potential injectivity	Utilize collected data and analyses to estimate potential permeability-thickness of target injection zone and identify boundary conditions that will affect injection estimates; assess well stimulation and completion scenarios to achieve target injection rates
Evaluate existing seismic	Existing regional seismic data could be used to validate the regional stratigraphic and structural framework. All available seismic attribute data should be integrated with the injection zone, structure, confining system and capacity evaluations. If existing seismic data is not available, it is recommended that a project developer wait to acquire data during the initial characterization stage—unless regional geology warrants information earlier in process
Prospective storage resources	Prospective storage volumes should be calculated utilizing acquired data, reporting resource volume ranges (low/medium/high) with identification of uncertainties in calculations. The reservoir evaluation should be used in calculation of prospective storage with all parameters and sources defined, such as “efficiency” calculations. Calculations should be reported assuming a maximum storage pressure and either an open or a closed system for brine displacement as endpoints. For more details for methods of calculation see NETL (2013)

Table 7.3 NETL guidelines for initial site characterization in terms of geoscientific aspects (after NETL 2013)

Element	Guidelines for initial characterization—geoscientific aspects
Geological	Develop site specific geologic baseline of qualified site(s) including type log/stratigraphic column; detailed correlation of reservoir architecture including injection intervals within the injection zone and potential confining zones within confining system; detailed structural maps; interpreted depositional model and facies distribution; porosity maps for potential injection intervals and zones; and porosity/permeability log transforms. This evaluation should be updated as additional information is acquired (seismic and well data). During initial characterization any additional data from a new well tests should also be integrated into previous analyses
Geochemical	Develop baseline of groundwater in all overlying aquifers using fluid and fluid level data collected in shallow aquifer formations in offset wells. If available, collect rock and fluid property data (composition, geochemistry, pH, conductivity, mineralogy) from the injection zone to model formation fluid-CO ₂ - rock reactions in the injection zone and at confining zone interfaces

(continued)

Table 7.3 (continued)

Element	Guidelines for initial characterization—geoscientific aspects
Geomechanical	Develop baselines for injection rates and pressures utilizing drilling data on formation strength and modeling. Analyze advanced logging suites from offset wells and characterization wells (if any exist) to identify faults and fractures. Analyze new or existing core to determine the existing stress state and assess the impact of changes in pore pressure on stress
Hydrogeological	Determine fluid compositions and injection zone flow units from new or offset well data, fluid samples, and hydrologic and other tests; integrate into dynamic injection zone models and compare to the existing hydrogeological model. Conduct multi-well tests where possible. Injection zone fluids and hydraulic tests should be further investigated during the site characterization phase and fluid samples should be collected if a new well is drilled or an existing well(s) is further tested
Flux baselines	Plan a monitoring system to establish baseline readings of near surface, ground level, and shallow subsurface fluxes. Baseline monitoring should be conducted during initial characterization and conducted for at least a year to account for changes in flux reading due to seasonal changes. Nearby urban, industrial or agricultural expansions and developments may require re-establishing a baseline prior to injection

discussed in Sects. 7.2–7.5 also have a special emphasis on some of the methods developed within the EU FP7 MUSTANG (www.co2mustang.eu) project that has been the starting point of this book. There is also focus on what can be defined as characterizing the dynamic properties of the site in terms of CO₂ transport and trapping (Sects. 7.3–7.5). In terms of building up the geological models and assigning their properties we refer to the number of example sites studied in the previously mentioned MUSTANG project and some of the related Deliverables (Erlström et al. 2010, 2011). A comprehensive site characterization for one of these sites, a research scale CO₂ injection site at Heletz, Israel, is summarized in Niemi et al. (2016), including demonstrating the use of old data from oil investigations and new data specifically collected for the purpose of CO₂ injection studies. Section 8.6 of this book that describes the Frio, USA CO₂ injection experiment also gives a good example of the relevant site characterization in the injection experiment scale. Other examples of thorough site characterization work can be seen in e.g. the US Regional Partnership Studies on CO₂ storage.

7.2 Geological Characterization

Katrina Edlmann, Christopher Ian McDermott and Christopher Juhlin

Geological characterization or construction of the static model of a CO₂ storage site uses data sets, such as cores, wireline logs, seismic and production data along with insight from outcrop analogues to characterise the geological architecture of the storage complex. The input data sources, in decreasing scale are:

1. Seismic data to determine the large scale 3D geometry of the site, combined with an understanding of the geological depositional environment, tectonic history and stratigraphy.
2. Geomechanical facies analysis where different tectonic settings exert different depositional process controls within the tectonic basin, which in turn influence CO₂ storage site suitability in terms of basin architecture, caprock architecture, reservoir quality, stress state, mechanical characteristics, fractures, burial depth, geothermal gradient, risk of orogenic modification, structural stability and preservation potential.
3. Wireline log data to provide information on the geology and stratigraphy, including reservoir and caprock thickness and distribution along with reservoir scale measurements of the petrophysical properties.
4. Production data to provide information on initial reservoir fluids and pressure, as well as possible flow barriers.
5. Core data to provide more detailed petrophysical information.

7.2.1 Large Scale Geology

It is necessary to characterise the geology of the storage complex at both local and regional scales. The local scale geological characterisation concentrates on geometry of the storage formation along with the caprock and overburden extent and structural compartmentalisation. The regional scale geology will identify basin wide CO₂ migration patterns and enable the bulk residual and solubility storage potential to be calculated.

7.2.1.1 Seismic Data

The primary data source for large scale geological characterization is seismic data. Acquiring such data, in its simplest form, involves a surface source generating seismic waves which propagate downwards and are reflected in the subsurface at geological boundaries. The reflections propagate upwards and are recorded on surface sensors as a function of time. Large amounts of data are normally acquired and processed. The processed data provide structural images of the subsurface where different reflections generally correspond to different subsurface lithologies. These processed images can be displayed in 2D or 3D, depending upon the acquisition geometries of the sources and receivers, and as a function of time or depth. If displayed as a function of depth, then the seismic velocity of the media needs to be estimated. This can be done by analyzing the data itself to provide a general estimate of the velocity function for the data set. However, it is also useful to have borehole logs and borehole seismic data to increase the accuracy of the estimated velocity function for the surface seismic data. Ideally, a 3D depth

converted image should be used for interpretation. In addition to the image, seismic attributes can be determined from the data which can aid in the interpretation. Examples of such attributes are reflection strength, changes in amplitude with offset (AVO) and instantaneous frequency (for further details see Sect. 8.2.2).

The amplitude of a reflected wave depends on the contrast in velocity and density at the boundary of the two media. Normally if the velocity increases the density will also increase, but there are also exceptions. It is the product of the velocity (v) and density (ρ) which controls the reflection amplitude and this product is known as the impedance (Z). For waves that impinge on a boundary between two media at right angles the reflection coefficient is usually defined as:

$$R = \frac{(Z_2 - Z_1)}{(Z_2 + Z_1)} \quad (7.2.1)$$

where Z_2 is impedance in the medium below the boundary and Z_1 is the impedance in the medium above the boundary. With this definition, reflections from interfaces in which the impedances increase below it will have a positive reflection coefficient and reflections for which the impedance decreases below it will have a negative one. This can be used to identify material boundaries. Hard limestones and tight sandstones, for example, generally have high impedances while soft shales and highly porous sandstones have low impedance. Coal layers have generally very low impedance.

An important consideration when interpreting seismic data is the data resolution, both in the vertical and horizontal directions. The reflection coefficient defined above assumes the recorded reflection waveform is from a single interface. However, if the layer is thin, the reflection at the base of the layer will interfere with the reflection off the top of the layer (Fig. 7.1). This interference may either decrease or increase the apparent reflection strength of the layer and it becomes difficult or impossible to separate the reflected signal from the top and bottom of the layer. When the two cannot be separated the vertical resolution limit of the data has been reached, this being governed by the velocity of the media and the frequency of the seismic waves propagating through it. This limit is generally defined as one quarter of the wavelength (λ) of the signals in the data. The wavelength is dependent upon the velocity of the media and the frequency (f) of the signal so the vertical resolution limit (λ_R) will be:

$$\lambda_R = \frac{v}{4f}. \quad (7.2.2)$$

The greater the frequency of the generated seismic waves the better the resolution. For a typical seismic survey the velocity of the media may average 3000 m/s and signal frequencies of 50 Hz may be generated. The resolution would then be 15 m. That is, layers thinner than 15 m cannot be resolved. Note that they will be detected by the seismic method, but one will not be able to quantitatively measure their thickness. The horizontal resolution also needs to be considered when

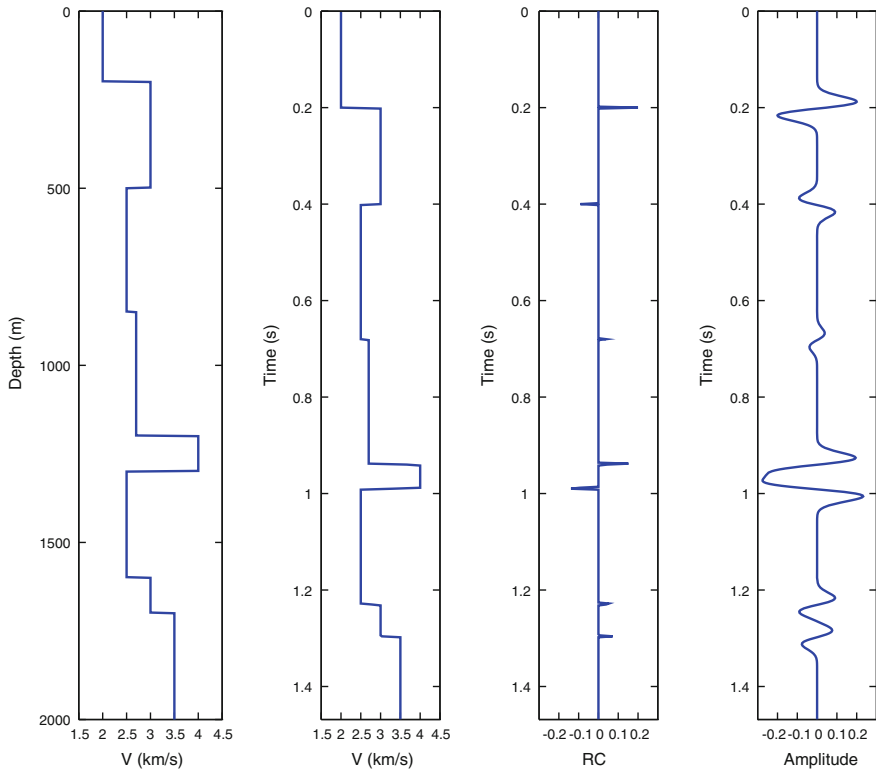


Fig. 7.1 Example of how reflections from interfaces close to one another interfere with one another. *Panel 1* shows the velocity as a function of depth, *panel 2* shows it as a function of time, *panel 3* shows the reflection coefficient as a function of time assuming that the density is constant, *panel 4* shows the resulting seismic response for a wavelet that has a dominant frequency of 30 Hz. Note how the reflections from the *top*, at the *bottom* of the high velocity layer at about 1250 m depth interfere with one another, producing a composite reflection

interpreting seismic data. Horizontal resolution will generally decrease as a function of depth due to spherical spreading of the wave fronts. In general, the horizontal resolution will be less than the vertical resolution.

There are many examples of how seismic data have been used to characterize CO₂ injection sites of different scales. Both depleted gas fields (e.g. Urosevic et al. 2010) and small scale saline aquifer sites (e.g. Alcalde et al. 2013; Doughty et al. 2008; Juhlin et al. 2007) have been characterized. In the Decatur project in Illinois, USA a relatively large 3D seismic survey was performed prior to injection of about 1 million tons of CO₂. For depleted oil and gas fields there will often exist previous seismic data, but of older vintage. Therefore it may be necessary to acquire new data, both for characterization and as baseline for future monitoring. For saline aquifer injection sites there will generally be limited previous seismic data available, especially if there are no overlying producing petroleum accumulations. In

most of these cases it will be necessary to acquire new 3D seismic data in order to properly characterize the site.

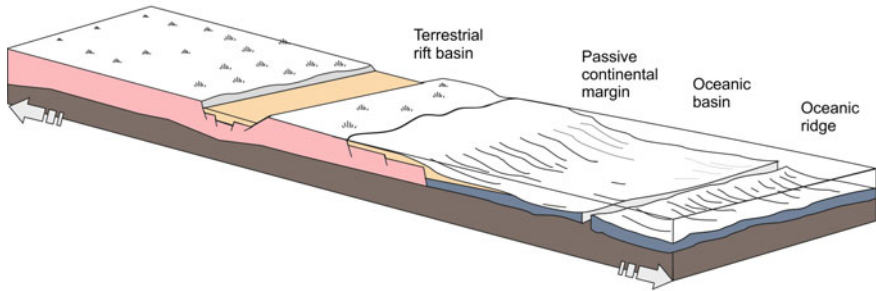
In spite of the resolution limits, a great deal of information about the subsurface structure can be gained from a seismic survey. The information content can be increased by combining the seismic data with borehole data and information on regional geology. Sedimentary processes in any given depositional environment will have a characteristic distribution of sediment types, termed facies, which can be utilized to provide input data for the large scale geology. These facies can often be identified in the seismic data. Combining the seismic data with an understanding of the depositional environment and regional geology can provide a more detailed picture of the subsurface geology.

7.2.1.2 Depositional Environments and Facies Analysis

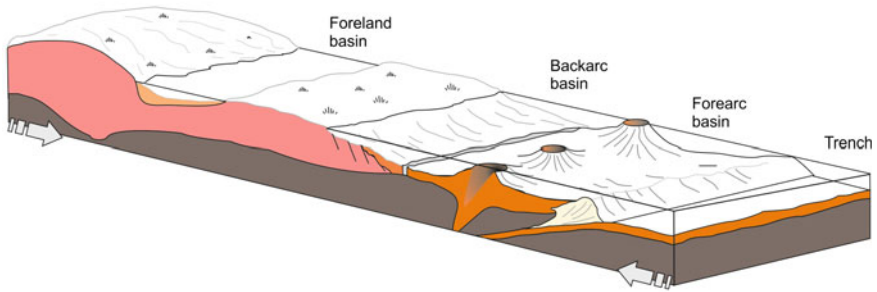
Different tectonic settings (Fig. 7.2) exert different depositional process controls within the tectonic basin. These in turn will influence the suitability of the CO₂ storage in terms of basin and caprock architecture, reservoir quality, stress state, mechanical characteristics, fracturing, burial depth, geothermal gradient, risk of orogenic modification, structural stability and preservation potential (Hallam 1981). The different tectonic settings include (i) extensional tectonics resulting in oceanic basins, passive continental margin basins and terrestrial rift basins; (ii) convergent tectonics resulting in trench basins, forearc basins, back arc basins and foreland basins and the (iii) wrench tectonics creating strike slip basins. Geological sedimentary deposits are not randomly formed, but control is exerted by the influence of tectonics over the depositional and structural processes. This leads to the formation of layers of strata which can be grouped together according to their engineering characteristics. By examining the typical characteristics of the geomechanical facies within the different tectonic settings, it is possible to compare and contrast the different tectonic settings to appraise global CO₂ storage opportunities and predict which tectonic settings will be the most suitable for CO₂ storage (Edlmann et al. 2014).

Using the geomechanical facies approach, inputs crucial to the primary CO₂ storage requirements of storage volume and storage security can be evaluated and graded as (i) good, (ii) moderate and (iii) poor, based on an assessment of their net contribution towards providing ideal CO₂ storage conditions. Work by Edlmann et al. (2014) show that foreland basins and passive continental margin basins are more likely to be suitable basins for CO₂ storage than other tectonic settings and should therefore be prioritized for investigation. Strike-slip basins, terrestrial rift basins and back arc basins are also suitable for CO₂ storage with oceanic basins and fore-arc basins being moderately suitable and trench basins unsuitable tectonic settings for CO₂ storage. The geomechanical facies approach is discussed in more detail in Chap. 9.

(A) Extensional tectonic system



(B) Compressional tectonic system



(C) Strike slip tectonic system

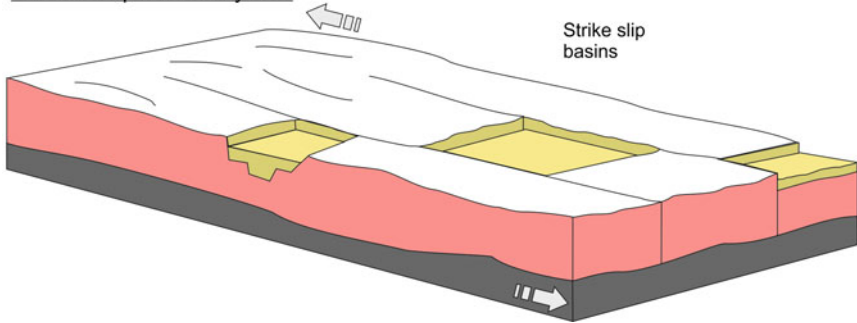


Fig. 7.2 Schematic of the basin types formed under the three primary tectonic settings

7.2.1.3 Wireline Logs

Wireline logs are continuous instrument measurements of the downhole formation where the physical properties of the formation rocks can be inferred from the instrument response. The direct wireline instruments include borehole imaging, electrical resistivity, acoustic response, natural radioactivity, radioactivity response, electrical potential, neutron magnetic resonance and calliper response. These allow the inference of lithology, bulk density, porosity, permeability, fluids type and

saturation, stress state, fracture network and mechanical strength. Wireline logs provide a continuous recording of parameters with depth and as such they are very useful for geological characterisation. They provide stratigraphic information through the reservoir and facilitate well to well correlations that can cover the whole field, where intervals of different wells are matched for similarity or characteristic log responses to lithological markers. The wireline logs are also used to provide a geological check to the seismic interpretation. Below some examples are given of what information can be obtained from wireline logs in terms of geological characterization.

To differentiate between the porous and permeable reservoir rocks and the non-permeable clays and shales and to indicate the shaliness of the rocks, the Spontaneous Potential (SP) log and the natural Gamma Ray (GR) are used. The Spontaneous Potential (SP) log shows the electrical potential (voltage) produced by the formation and drilling fluids along with the shales. The natural Gamma Ray (GR) in turn indicates the natural radioactivity of the formation, most of which is within shales as radioactive elements tend to concentrate in clays and shales.

The LithoDensity log measures the density and the photoelectric absorption index of a formation. The density log primarily responds to porosity and pore fluid and secondarily to the rock matrix (lithology) properties, the photoelectric absorption primarily responds to the rock matrix properties and secondarily to the porosity and pore fluid. From these a clear indication of the likely lithology can be obtained.

The neutron, density and sonic logs can be used to determine lithology through the use of crossplots, where various combination of logs respond to lithology. The neutron-density crossplot allows the identification of sandstone, limestone and dolomite. The sonic-density crossplot is particularly useful to identify evaporates. The sonic-neutron and the density-photoelectric crossplots are also useful at facilitating the identification of sandstone, limestone and dolomite (Schlumberger 1991).

7.2.2 Reservoir Petrophysics from Well Log-Scale Observations

Commonly determined petrophysical parameters from logging tools include:

Shale Content: There are primarily two logs that are used in shale identification:

1. The Spontaneous potential (SP) log which measures the difference between electrical potential of a movable electrode in the borehole and the electrical potential of a fixed surface electrode indicates the presence of shales, where shales usually show a straight line on the SP log trace and porous formations will deviated from this shale baseline.
2. The gamma ray log (GR) which records the natural radioactivity of the formation which depends on the concentration of potassium, thorium and uranium, which tend to concentrate in clays and shales.

Rock Porosity: Rock porosity can be obtained from the sonic, density and neutron logs.

1. The sonic log is a recording versus depth of the time taken for a sound wave to traverse 1 ft of formation known as the interval transit time which is a function of lithology and porosity.
2. The density log response is determined by the electron density of the formation which is related to true bulk density which depends on the density of the rock matrix, porosity and fluid density.
3. The neutron log reflects primarily the amount of hydrogen in the formation which is due to the fact that neutrons lose most energy when they collide with a hydrogen nucleus.

Lithology Determination: the measurements of the neutron, density and sonic logs depend not only on porosity but also on the formation lithology and crossplots can be used to demonstrate how various combinations of logs respond to lithology.

Stratigraphic Determination: All logs will reflect sedimentary features; however their vertical resolution is not sufficient to detect thin beds. The dip meter tool is designed to provide detailed downhole information and enhances resolution of strata based on micro resistivity measurements.

Fracture Determination: The array sonic tool can be used to identify fracture zones, where high signal strength at the receiver suggests a competent rock. The calliper tool which measures the borehole shape can also identify breakout or fractured areas within the formation.

Elastic Constants: Dynamic elastic constants can be determined from the measurement of elastic wave velocities from the sonic logging tools.

7.2.3 Reservoir Petrophysics—Core-to-Pore Scale Observations

The physics of deposition and the wide range of geological environments lead to a vast range in geological heterogeneities at different scales of investigation. Within the reservoir analysis there are three primary scales to consider:

- The pore scale, which considers the grain and pore size distribution and shape and is at the micron to millimetre scale, where the laminae scale geological structures are dominant.
- The core scale, where the geological structure of the rock becomes apparent. This is the centimetre scale and depositional bedding structures are dominant and the heterogeneity of the system has increased.
- The reservoir/log scale, where heterogeneities are on the meter to kilometre scale.

These different scales of measurement can, to a certain extent, be addressed by tying scales of data to each other as a calibration. For example, high resolution core data can be used to refine wireline data.

There is a wide range of core analysis that provide petrophysical input data. Typically, a rotary coring bit is used to recover the core, which is hollow in the centre, called the core barrel, where the core is stored and retrieved. The process of coring is expensive and normally only performed through the reservoir interval. Side wall cores of around 1 in. (note; 1 in. = 2.54 cm) in diameter can also be obtained directly from the reservoir.

Any core plug samples are likely to be fully saturated with the drilling fluids. The coring process will also damage the rock, which is not always discernible and there will be a stress release during retrieval which in extreme circumstance may mean the rock is no longer representative of the in situ rock properties. Damage will occur through stress, pore pressure and temperature release and exposure to non-native fluids. This will have an impact on the petrophysical measurements to be performed on the cores. Ideally experiments should recreate the in situ stress conditions, but this is not practically possible and must be considered during analysis, paying attention to the importance of a particular damage mechanism to the rock property being measured, for example a mechanism that changes the structure of the pore fill material will have a great impact on permeability and less so on the mechanical property of the rock.

Routine core analysis procedure involves initial core gamma logging to provide a tie between core depth and logging depth. Then the core plugs are taken and porosity, permeability and saturation are measured. The core is then sliced and core photographs are taken in both white and ultra violet light for both documentation and core description. For more complex reservoir measurement, Special Core Analysis can be undertaken which provides capillary pressure, relative permeability, electrical properties, wettability and nuclear magnetic resonance. In addition rock mechanical testing, miscible gas and chemical flooding and further detailed thin section petrography can be conducted to provide as much information as possible about the rocks.

7.3 Dynamic Characterization—Hydraulic, Tracer and Thermal Properties

Jesus Carrera, Alexandru Tatomir, Iulia Ghergut, Martin Sauter and Jacob Bensabat

This section deals with field tests performed to characterize the hydrodynamic properties of the aquifer prior to actual injection. The most important parameters for the purpose of CO₂ storage are permeability, porosity and geomechanical properties. Permeability of the aquifer controls the injection pressure, the rate at which CO₂ will dissolve into the native brine, and the regional pressure buildup. Permeability of the caprock, together with entry pressure, controls the efficacy of the caprock in containing the injected CO₂. It also controls the migration of brine to overlying water bodies. Porosity determines the storage capacity of the aquifer.

Geomechanical properties control the maximum sustainable injection pressure (rock strength) and the associated deformation (Young's modulus and Poisson ratio). In addition to these parameters, it is also necessary to characterize retention properties, which control capillary trapping and, reactive surface, which controls the rate of chemical reactions.

The evaluation of these properties at the core scale has been described in Chap. 6. However, as discussed in Chap. 5, core scale parameters are rarely the representative ones at the field scale. Heterogeneity, notably fractures or high permeability channels cause small scale (laboratory) parameters to be different from those effective at the field scale. Evaluating these requires field tests. The types of field tests that can and are being used for characterizing CO₂ storage sites include:

1. Hydraulic tests
2. Tracer tests, using both conservative and reactive tracers
3. Thermal tests
4. High pressure injection tests
5. CO₂ injection tests.

The first three of these are described in the following sections while the fourth and fifth type of test are discussed in Sects. 7.4 and 7.5.

7.3.1 Hydraulic Tests

Jesus Carrera and Alexandru Tatomir

For almost a century, hydraulic tests have successfully been relied upon for diagnosing aquifer characteristics based on the evaluation of aquifer response data. These tests are commonly performed by pumping or injecting water out of a well while measuring the changes in water level (drawdown) in this well or, if present, in nearby observation wells. The drawdown can be analyzed using various models to obtain estimates of the aquifer parameters, which characterize the transmissive and storage characteristics of the aquifer and the flow system boundaries (Fig. 7.3).

7.3.1.1 Conventional Pumping Tests

The conventional pumping test is performed by pumping an ideally constant flow rate from a fully penetrating well. Hydraulic parameters are determined by matching the measured time-drawdown curves with known type curves of appropriate models or solutions to the groundwater flow equation. The solutions for the type curves require simplifying assumptions such as homogeneity and infinite areal extent. Water is assumed to be released instantaneously from storage with decline of hydraulic head.

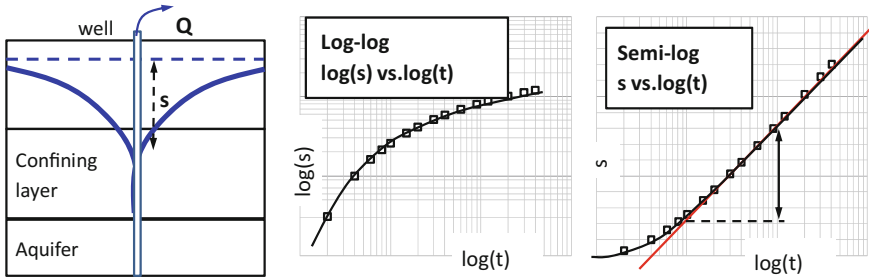


Fig. 7.3 Hydraulic tests are performed by pumping (or injecting) a flow rate Q from a well, and measuring the resulting drawdowns. (s) Parameters are obtained by fitting a model to measurements, which is frequently done graphically using log-log or semi-log graphs

The simplest and most widely used analytical solution to well hydraulics is the one of Theis (1935), which yields the aquifer response to constant pumping from a fully penetrating well in a confined aquifer (Fig. 7.3). The influence of pumping extends radially from the well with time, according to:

$$s = \frac{Q}{4\pi T} \int_u^\infty \frac{e^{-y}}{y} dy = \frac{Q}{4\pi T} W(u) \tag{7.3.1}$$

where s is drawdown, Q is pumping rate, S is storage coefficient, T is transmissivity, $u = Sr^2/4Tt$, and $W(u)$, implicitly defined by Eq. (7.3.1) is called “well function”.

A relevant and enlightening approximation to the well function was proposed by Jacob and Cooper (1946):

$$s = \frac{2.3Q}{4\pi T} \log\left(\frac{2.25Tt}{Sr^2}\right) = \frac{2.3Q}{2\pi T} \log\left(\frac{R}{r}\right) = \frac{2.3Q}{4\pi T} \log\left(\frac{t}{t_0}\right) \tag{7.3.2}$$

where R is the radius of influence $R = \sqrt{2.25Tt/S}$ and $t_0 = Sr^2/2.25T$ is the response time.

Equation 7.3.2 shows two essential properties of the aquifer response to pumping (or injection) (Fig. 7.4). First, when drawdown is plotted versus $\log t$, it tends to display a straight line whose slope m is inversely proportional to transmissivity and whose intercept is t_0 . From these, transmissivity and storativity can be obtained as:

$$T = \frac{2.3Q}{4\pi m} = 0.183 \frac{Q}{m} \tag{7.3.3}$$

$$S = \frac{2.25Tt_0}{r^2} \tag{7.3.4}$$

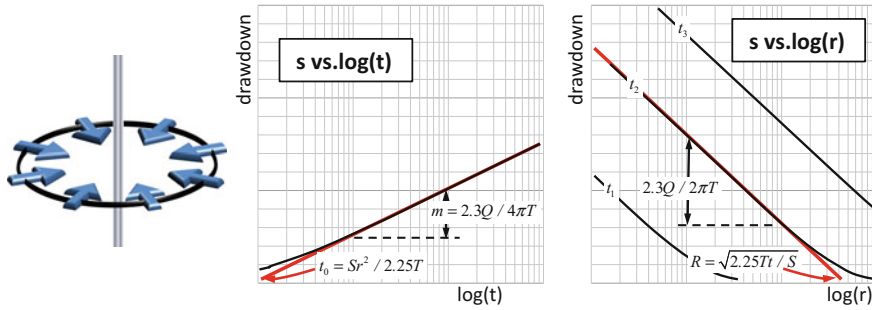


Fig. 7.4 Under radial flow conditions, drawdowns tend to plot as a straight line when plotted either versus $\log(t)$, which allows defining the response time t_0 , or versus $\log(r)$, which allows defining the radius of influence, R . As time grows, so does the cone of depression, but its shape does not change

The second interesting property of Eq. (7.3.2) is that drawdown will also plot as a straight line, with slope equal to $2.3Q/2\pi T$, when plotted versus $\log r$. That is, pumping causes a cone of depression that is displaced downwards (i.e. its pressure drops) as time evolves, but whose shape does not change with time. The cone is always centered at the well and its external radius evolves with R . As we shall see, this property (unchanged shape) remains true even in heterogeneous aquifers.

Data can be represented in several ways to obtain the maximum information from the drawdown (pressure buildup, in the case of injection) data. The traditional method consists of plotting drawdown versus time, both in logarithmic scale (Log-log plot, Fig. 7.3). Ideally, data should be identical to Theis solution; allowing superposition and estimation of T and S from the shift in the vertical and horizontal axes, respectively. Perhaps the simplest representation consists of plotting drawdown versus logarithm of time (semi-log plot). In this case, data should tend to form a straight line for large times if flow is radial (Cooper–Jacob approximation). Transmissivity can be obtained from the slope of this line, whilst the storage coefficient results from its intersection with the $\log t$ axis.

The fact that drawdown versus $\log(t)$ tends to a straight line under radial flow conditions, prompted Chow (1952) to propose using the derivative of drawdown with respect to log time $\partial s / \partial \ln t = t \partial s / \partial t$ as an interpretation method. The concept was generalized by Bourdet and his colleagues (Bourdet et al. 1983, 1989). They analyzed the behaviour of the log-derivative for a large number of classical models of flow around a pumping well. Doing so, they showed that the joint use of the drawdown and its log-derivative can be highly informative and developed the concept of diagnostic plots. A diagnostic plot (Bourdet et al. 1983) is a simultaneous plot of the drawdown and the logarithmic derivative of the drawdown as a function of time in log–log or semi-log scales (Fig. 7.5). This plot is used to facilitate the identification of the conceptual model best suited to interpret the data. Detailed explanations on the method are provided by Bourdet et al. (1983) and Renard et al. (2009). We will discuss them in some detail later. Prior to that, it is convenient to discuss recovery tests.

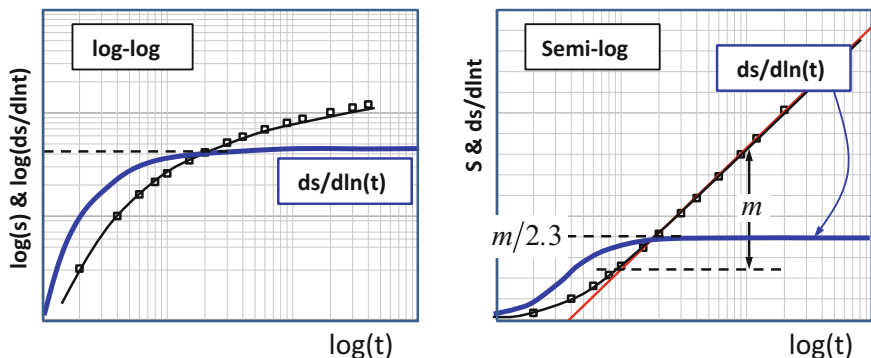


Fig. 7.5 Diagnostic plots include drawdown and derivative graphs. Both log–log (*left*) and semi log (*right*) graphs are useful. In the pure radial flow case, the derivative tends to a constant ($m/2.3$). The 2.3 factor reflects that derivatives are taken with respect to $\ln(t)$, while the slope m is obtained from the semi-log graph, where the logarithm is decimal

7.3.1.2 Recovery Tests: Theis and Agarwal Methods

Recovery refers to the return of pressure to its natural state. Strictly speaking, it is a “passive” test. However, data collected during recovery may be more informative about the properties of the aquifer than those collected during pumping (or injection). Most aquifer test theory is based on the assumption that the pumping (or injection) rate is constant, which is rarely true. Pumping rate is variable, especially during the early portion of the test, which is often the most informative about aquifer properties. As such early time may not be very reliable. Instead, recovery only requires turning the pump off, which makes these data more reliable.

Solutions to recovery can be obtained in several ways. They generally rely on superposition. The traditional Theis recovery method (Horner method in the petroleum literature) consists of superimposing the head response to pumping and to an injection that starts at the end of pumping (Fig. 7.6). A simple illustration of the concept can be obtained using Jacob approximation (Eq. 7.3.2), which leads to

$$s_R = s_P(t) - s_P(t - t_P) = \frac{2.3Q}{4\pi T} \left(\log\left(\frac{t}{t_0}\right) - \log\left(\frac{t - t_P}{t_0}\right) \right) = \frac{2.3Q}{4\pi T} \log\left(\frac{t}{t - t_P}\right) \tag{7.3.5}$$

where s_R and s_P are the recovery and pumping drawdowns, respectively. This equation, points that recovery data will also tend to a straight line when plotted versus $\log(t/t - t_P)$. This leads to Theis recovery method that consists of deriving transmissivity from such slope using Eq. (7.3.3). This estimate of transmissivity is quite robust (Willmann et al. 2007). Notice that this approach ignores the estimation of storativity, which indeed reflects that late time recovery is not sensitive to storativity.

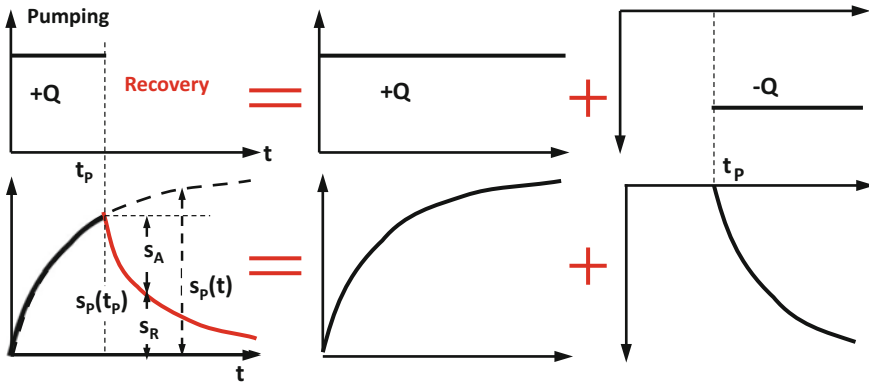


Fig. 7.6 Superposition to obtain recovery plots. This recovery method consists of plotting s_R versus $t_p(t - t_p)$, which results from Eq. (7.3.5). Agarwal method consists of plotting $s_p(t_p) - s_R$ versus $t_p^3(t - t_p)/t$, which should yield a graph very similar to that obtained with a constant pumping rate, see Eq. (7.3.6) and makes it a very attractive method

This limitation can be overcome using Agarwal method, which is a somewhat more sophisticated version of recovery that consists of computing head recovery (i.e., drawdown at the end of pumping minus drawdown during recovery, often termed Agarwal’s drawdown) from the fact that drawdown during recovery is directly $s_p(t)$ minus $s_p(t - t_p)$. Using Eq. (7.3.2) to approximate all terms involved, yields:

$$s_A = s_p(t_p) - s_R(t) = s_p(t_p) - (s_p(t) - s_p(t - t_p)) = \frac{2.3Q}{4\pi T} \log\left(\frac{t_p(t - t_p)}{t_0 \cdot t}\right) \tag{7.3.6}$$

Notice that this solution is identical to the one of Eq. (7.3.2), except that time is changed by Agarwal’s time $t_A = t_p(t - t_p)/t$. Therefore, Agarwal’s drawdown should be very similar to the one caused by a constant pumping rate, provided that t_A is used instead of t . As it turns out, the solution is approximately valid well beyond the Cooper–Jacob solution used here. The only limitations are that pumping should be constant for some time prior to the stop in pumping and that, obviously, Agarwal’s time is bound by pumping duration. In fact, the solution is not valid for times close to t_p . It is clear that Agarwal’s should be the method of choice, as it only requires careful monitoring of recovery.

7.3.1.3 Effect of Heterogeneity

Heterogeneity is arguably the most ubiquitous feature of natural media. As such, heterogeneity must be acknowledged when dealing with permeable media (recall extensive discussion in Chap. 5). In the hydraulic testing context, two extreme

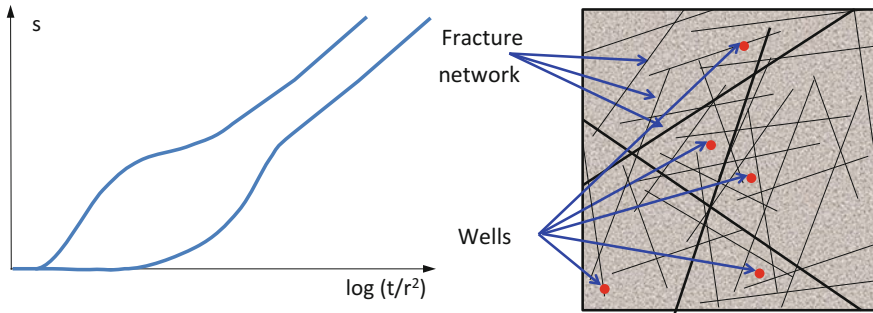


Fig. 7.7 Large scale transmissivity is controlled by preferential flow paths (long, permeable, well connected fractures). The probability of intersecting these fractures is low. So that transmissivity derived from injectivity or short term tests tends to be much smaller. Large scale transmissivity may be derived from the slope of long term tests, which is the same regardless of whether the pumping or observation wells are located in high or low permeability areas. Local features are reflected in the early portion of the drawdown curve

attitudes can be adopted: trying to identify heterogeneity (see, e.g., Yeh et al. 2000; Alcolea et al. 2006) or seeking effective parameters.

The former requires many observation points and several pumping wells, which can be realistic in CO₂ storage project. The latter has been the focus of much research and numerous methods have been developed. All these methods yield similar results (Sánchez-Vila et al. 1995), but no one is generally accepted as best.

An important result from this type of work is the finding that the equivalent transmissivity can be larger than the geometric average of point T values, whenever high T values are well connected (Sánchez-Vila et al. 1996). This is expected to be the rule, rather than the exception (think of fractured media, sedimentary materials, with coarse sediments paleochannels, etc.). An explanation for this “scale effect” is given in Fig. 7.7. Most wells will not intersect the most conductive fractures this yielding relatively small transmissivities. If many wells were available and computed their geometric average, T_G (the traditional effective transmissivity for 2D flow), it would be concluded that the aquifer transmissivity is small. In reality, fluids would flow through the fractures. Therefore, one should expect T_{eq} to be larger than T_G . In fact, Knudby and Carrera (2005) use the ratio T_{eq}/T_G to define connectivity. The question is whether one can estimate equivalent transmissivity from field data, which is addressed below.

The value of transmissivity one obtains from a pump test depends on whether the test is interpreted using Theis, Jacob or Thiem method. That is, the resulting transmissivity is as much a property of the real medium as of the adopted model. The question is whether one can draw any general conclusion from such interpretation. This question was addressed by Meier et al. (1998), who simulated pumping tests in heterogeneous media by imposing a constant flow rate at one node and observing drawdown at all other nodes (Fig. 7.8). They then interpreted the drawdown curves at all nodes using Jacob’s methods. They found:

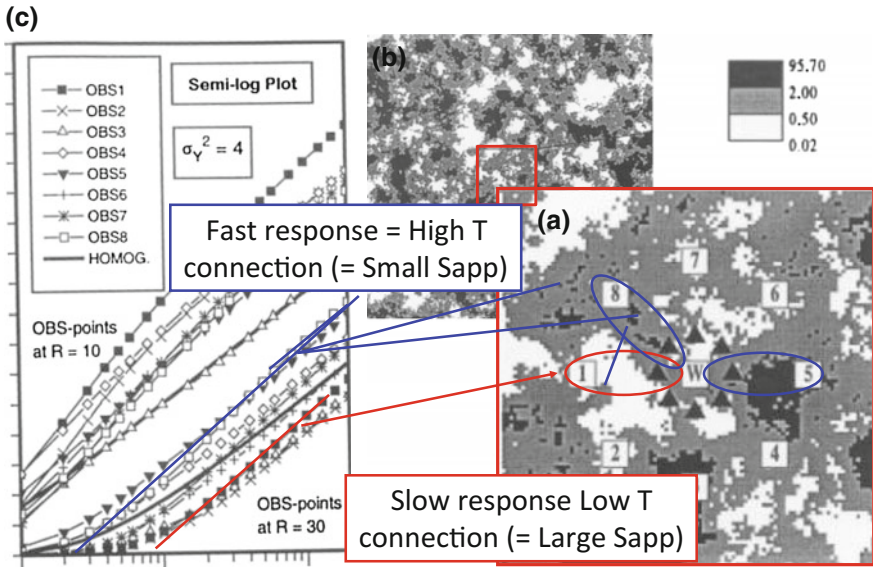


Fig. 7.8 Simulations of Meier et al. (1998) to show the effect of heterogeneity on pumping tests interpretation. **a** Transmissivity field; **b** local region around the pumping well with a few observation points; **c** semi-log drawdown plots. Note that all curves display the same late time slope (i.e., yield the same T), but response times (t_0) are highly variable (i.e., yield equally variable S)

1. The resulting estimated transmissivities were identical at every mode. That is, T estimated with Jacob’s method is independent of the location of the observation point.
2. The estimated transmissivity is identical to the equivalent transmissivity for parallel or radial flow.
3. Estimated storage coefficient reflects not only the actual storage coefficient, which was assumed constant, but also the degree of connection (high T) between the pumping well and the observation point.

In summary, conventional tests interpreted using Jacob method will yield highly reliable values of effective transmissivity for radial distances given by R in Eq. (7.3.2) or Fig. 7.4. Therefore, returning to Fig. 7.7, the important point is to make the test long enough to make sure that the fracture network is effectively tested. Unfortunately, the value obtained for storage coefficient is much less reliable, as it reflects the connectivity between pumping and observation well.

7.3.1.4 Perturbations to the Conventional Case

Up to here, we have analyzed the basic Theis case. In practice, a number of perturbations affect this basic theory: wellbore storage may not be negligible; flow may not be radial (e.g., because of fractures or leakage from the caprock), storage may not be released instantaneously; test response may be affected by the presence of boundaries, etc. In the following, and for the purpose of illustration, we discuss these effects.

Wellbore Storage: Theis (1935) neglected the volume of water stored in the well. This assumption may not be valid if the diameter of the well is large (i.e., if the volume of water stored in the well is large compared to the volume of water pumped during the observation interval). Under these conditions, at the beginning of the test, pumped water comes mostly from the well, rather than from the formation. Therefore, drawdown at the well equals $S_w = Q_t/A_w$, where A_w is the open area of the well. That is, the well acts as a deposit, which implies that drawdowns will plot as a straight line in arithmetic scale, and both drawdowns and their logarithmic derivative will also plot as a straight line with slope equal to 1 in the log-log plot (Fig. 7.9). Eventually, the drawdown becomes large enough to drive water towards the pumping well, so that Theis solution becomes valid again.

Boundary Effects: Theis (1935) assumed the aquifer to be infinite. Real aquifers are not. The drawdown cone will eventually reach some boundary. This is especially relevant for deep formations which may be compartmentalized (i.e., separated by no-flow boundaries) or intersected by permeable faults connecting the aquifer to another more permeable water body (effectively becoming a prescribed head boundary). The effect of these boundaries can be easily approximated using image wells. An image well is a virtual well located symmetrically to the pumping well with respect to the boundary. If water is injected at the image well with the same flow rate as the pumping well, drawdowns along the boundary caused by the pumping well will be compensated by head buildups caused by the image well. As a result, the boundary will indeed act as a zero drawdown boundary. Elsewhere within the aquifer, observation wells will first notice the effect of the pumping well, with a response analogous to that displayed in Fig. 7.3. Eventually, they will also notice the effect of injection at

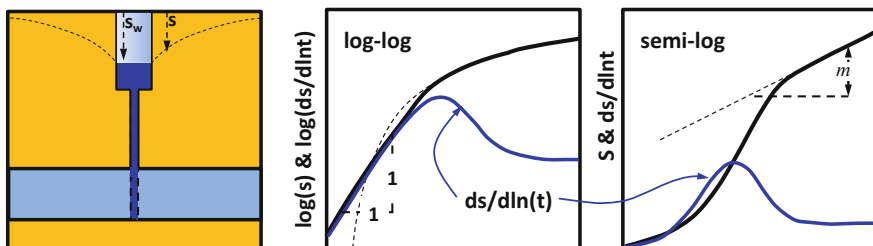


Fig. 7.9 Illustration of well bore storage effects. Well bore storage affects the shape of the response curves while Q_t is comparable to $A_w S_w$ —during this period, both drawdown and derivative plots display a straight line with slope equal to 1, in log–log scale. In semi-log scale, the drawdown curve displays a concave shape, while the derivative curve displays a maximum

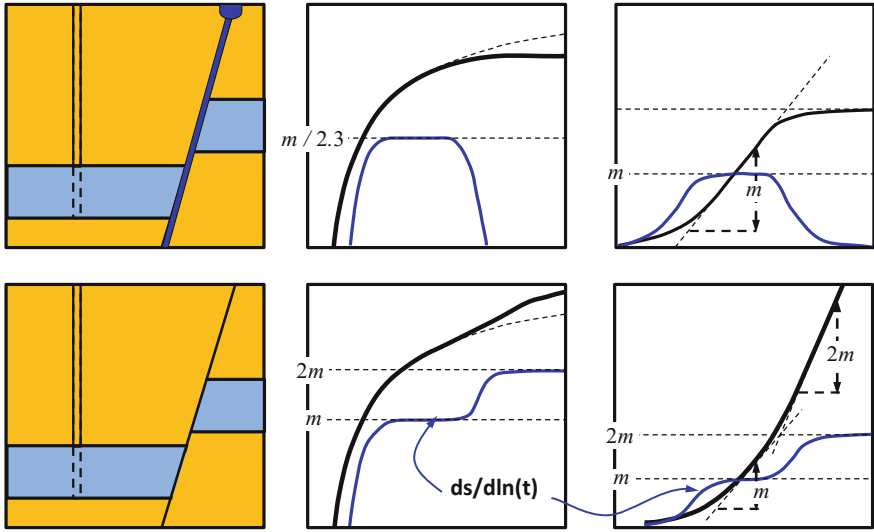


Fig. 7.10 Illustration of boundary effects. A linear prescribed head boundary (e.g., a high transmissivity fault connected to a constant head water body) can be identified by a zero derivative (drawdown becomes constant). If that fault does not allow flow-through, the derivative is multiplied by a factor of 2

the image well, which will cause the drawdown to become constant. Therefore, drawdown plots (Fig. 7.10, top) are characterized by a constant drawdown (the logarithmic derivative goes down as a straight line in the log–log plot).

If the image well is pumped with the same flow rate as the pumping well, flux across the boundary will be compensated by superposition. As a result the boundary effectively acts as a no-flow boundary. In this case, observation wells will also first notice the effect of the pumping well, but the image well, which is also pumping, will cause the drawdown to increase its rate. In fact, by superimposing the solutions to pumping and image wells, it is easy to demonstrate that drawdown plots (Fig. 7.10, bottom) are characterized by a sudden duplication in the slope of the drawdown curve in the semi-log plot or by a step increase the logarithmic derivative. In fact, distance to the image well can be derived from the time at which the effect of the boundary becomes noticeable, using it in the equation for R in Eq. 7.3.2.

More complex configurations of boundaries can be reproduced with several image wells. A case of special importance for CO₂ storage is the one of a close aquifer (i.e., full compartmentalization). In this case, by the time the effect of pumping has reached the whole aquifer, the compartment starts acting as a deposit. That is, drawdowns will tend to grow linearly with time, similar to what was described in the wellbore storage case. The slope will now be equal to $Q/(A \cdot S)$, where A is now the area of the compartment.

Leaky Aquifers: Theis (1935) assumed the aquifer to be confined by perfectly impervious confining layers. In reality, Confining layers over- and underlying an

aquifer are never completely impermeable, they are somewhat “leaky”. When a well in a leaky aquifer is pumped, water is withdrawn not only from the aquifer, but also from the over- and underlying layers, thereby creating a hydraulic gradient also in the aquitard. The flow is usually assumed to be vertical in the aquitard and horizontal in the aquifer (Kruseman and De Ridder 1994).

Leaky aquifers are especially relevant for CO₂ storage, because it is leakage across the caprock what will cause pressure buildup in the aquifer to be bounded. The effect of leakage is a slowdown in the rate of head drop, so that the derivative is also reduced (similar to the fixed head boundary, Fig. 7.10, but depending on the aquifer beyond the confining layer, drawdowns may eventually increase). The traditional solution for the leaky aquifer is that of Hantush and Jacob (1955), who neglected aquitard storage. The full solution was derived by Neuman and Witherspoon (1969).

7.3.1.5 Flow Dimensions

Everything discussed up to here, except the leaky aquifer case, was based on the assumption that flow is radial towards the pumping well (or at least that flow is two dimensional). In reality flow needs not be 2D (see Fig. 7.11). Flow will be 1D along a vertical fracture intersecting the well or 3D when pumping from a short interval in a very thick aquifer. Since the extent of the drawdown cone grows as $t^{1/2}$, its volume will grow as $t^{d/2}$. Therefore, the logarithmic derivative will tend to become straight with a slope equal to $1 - d/2$ in log–log plot. That is, if flow is 1D, the logarithmic derivative will tend to display a 0.5 slope. If flow is 3D, this slope will be -0.5 . Alternatively the dimension can be derived from this slope m , as $d = 2 \cdot (1 - m)$ (recall that this is the slope of the logarithmic derivative in log–log scale, not to confuse with the drawdown slope in semi-log scale).

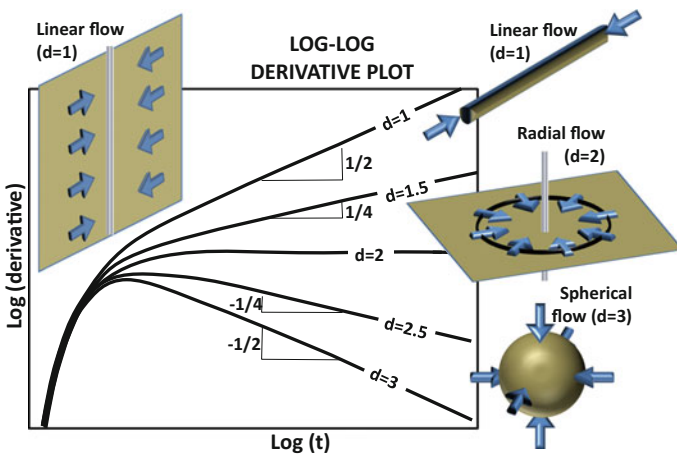


Fig. 7.11 Flow dimension effects

The surprising observation is that the resulting dimension is often non-integer. A body of literature has been developed to address this issue. The fact that the volume of the drawdown cone increases with a non-integer dimension may reflect a fractal connectivity pattern, which is not surprising in fractured media.

7.3.2 Tracer Methods for Characterization of the CO₂ Storage Sites

Alexandru Tatomir, Iulia Ghergut and Martin Sauter

Tracer testing can be defined as the injection into the hydro-geological system of one or more tracers, which usually are chemical compounds, but which can also be energy/temperature, viruses, DNA, etc. Tracer methods are commonly used to study the flow, transport and reactions of fluids and components in regions which are difficult to access and may extend over a wide range of length scales, like in the case of CO₂ storage reservoirs. Tracer methods are suited both for site characterization before CO₂ injection and for monitoring and verification purposes during and after CO₂ injection. The theoretical background of the tracer methods is well developed from the fields of hydrogeology and petroleum engineering. However, for geological storage of CO₂, new challenges arise due to the complex phase behaviour and the range of trapping mechanisms (i.e. structural, residual, solubility and mineral trapping).

The CO₂ storage reservoirs, as well as other technology-relevant geo-reservoirs in the realm of energy production (such as geological formations potentially suitable for spent-radionuclide disposal, gas storage or geothermal energy utilization) contain several fluid and solid phases, as well as mobile and immobile-fluid regions. The nature of utilization of the reservoir, the volumes and interfacial areas of the fluid phases and/or fluid regions, and the processes occurring within the phases are the factors which determine the lifetime of the reservoir. The lifetime of a geo-reservoir subject to a particular utilization can be subdivided and categorized into a hydraulic lifetime, a geomechanical, a hydrogeochemical, and a thermal lifetime. Figure 7.12 schematically illustrates the potential uses of tracer tests to answer fundamental questions related to each lifetime category and the complementarity that exists between the tracer test types. The tracer tests can be performed as single-well injection withdrawal (SWIW), or simply push-pull, tests, or in inter-well configurations. SWIW involves the injection and abstraction of tracer in one well, whereas inter-well testing requires two or multiple wells.

The concept of reservoir lifetime, transferred from the field of geothermal reservoirs, refers to an integral description of the reservoir properties and their change with time due to natural or anthropogenic factors, such as management by wells or CO₂ injection. The key parameters controlling the storage performance are the fluid flow pathways, the reservoir boundaries and hydrogeomechanical integrity, the storage capacity of the reservoir, the heat exchange areas (if existing) and fluid-rock and fluid-fluid interface areas. In designing and dimensioning tracer tests,

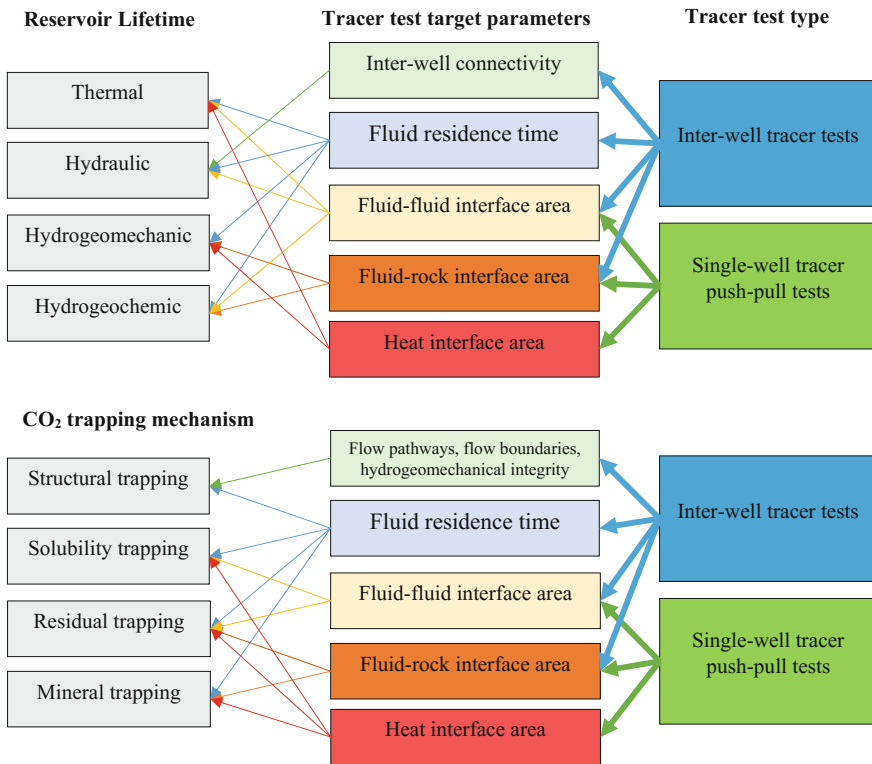


Fig. 7.12 Overview of reservoir lifetime categories (*upper left*) and CO₂ trapping mechanism (*lower left*), the target parameters which can be determined by the tracer tests (*middle*), and the respective tracer methods suitable for measuring them (*right*)

one has to consider that not every test design and any tracer species can be equally sensitive with regard to every fluid transport parameter. Therefore, when referring to tracer sensitivity and applicability range a certain complementarity exists between (Fig. 7.12):

1. Single-well and inter-well methods,
2. Equilibrium and non-equilibrium (kinetic exchange processes),
3. Volume (e.g. fluid phase saturation) and area parameters (e.g. fluid-fluid interfaces, fluid-rock interfaces).

7.3.2.1 Chemical Tracer Types

There is a wide spectrum of tracer applications, capturing various underlying processes and physico-chemical and biological properties, as illustrated in Table 7.4. Depending on their physicochemical and chemical behaviour, tracers can

Table 7.4 Compilation of tracers used for the characterization of geological systems (Schaffer 2013)

Tracer type	Injection phase	Application target parameters	Underlying processes	Exemplary compound classes	Most relevant tracer properties
Conservative					
<i>Conservative tracers</i>					
Ionic tracers	aq.	Hydromechanical properties (porosity, dispersion, matrix diffusion, arrival times)	None	Organic and inorganic anions (salts, fluorescent dyes)	Anionic, highly water-soluble, non-sorptive, low log D , low pK_a
Tritium tracers			None	Isotopically labeled water	Molecular weight $>18 \text{ g mol}^{-1}$
scCO ₂ plume marker	Non-aq.	Plume migration, arrival times	None	Perfluorocarbons (McCallum et al. 2005 [56])	Inert, non-polar (no partitioning into water)
Temperature (heating/cooling)	aq. (non-aq.)	Groundwater flow, thermal conductivity	Thermal conduction, advection/convection	None	
Pressure	aq. (non-aq.) (gas.)	Permeability, hydraulic conductivity, leakage, arrival times	Pressure stimulation/response	None	
<i>Colloidal tracers (particle tracers)</i>					
Microorganisms	aq.	Hydraulic connection, groundwater drift, mixing, transport of microorganisms	None, (adsorption, coagulation size exclusion)	Bacteria, bacteriophages, yeasts, animal viruses, colored or fluorescently labeled spores (<i>Lycopodium clavatum</i>) (Keswick et al. 1982 [41], Becker et al. 2003 [7])	(continued)

Table 7.4 (continued)

Tracer type	Injection phase	Application target parameters	Underlying processes	Exemplary compound classes	Most relevant tracer properties
Microspheres/nanoparticles)	aq.	Hydraulic connection, groundwater drift, mixing	None, (adsorption, coagulation, size exclusion)	Fluorescently labeled polystyrene or latex microspheres (Becker et al. 1999 [6], 2003 [7]), artificial DNA labeled microspheres (Sharma et al. 2012 [80]), fluorescent silica nanobeads (Agenet et al. 2011 [1])	
Retardation					
<i>Partitioning tracers (equilibrium tracers)</i>					
Sorptive tracers	aq.	Organic carbon content, retardation, (degradation)	Non-ionic sorption processes, (degradation)	Organic, hydrophobic compounds	Neutral molecules, moderate log K_{ow}
Ion exchange tracers	aq.	Surface charge, ionic strength, exchange area, retardation, (degradation)	Cation exchange, (anion exchange)	Inorganic (Dean et al. 2012 [17]) and organic cations (bases) (Leecaster et al. 2012 [46]; Reimus et al. 2012 [72])	Ionic molecules, low log D , high pK_a
Interfacial tracers	aq.	Interfacial area between immiscible phases	Adsorption on interface	Liquid/liquid interface (anionic) surfactants (Saripalli et al. 1997 [74], 1998 [73]), liquid/gas interface: high molecular weight alcohols (Kim et al. 1998 [42]; Rao et al. 2000 [70])	Amphiphil, ions with long alkyl chain or other non-polar substructures
Volume-sensitive tracers	aq. non-aq., gas.	Residual saturation of two phases	Partitioning between two phase volumes	Alcohols (Annable et al. 1998 [3]), phenols (Bennett and Larter 1997 [10]), (noble) gases (Vulava et al. 2002 [91]), fluorocarbons (Deeds et al. 1999 [18]), radioisotopes (Hunkeler et al. 1997 [34]; Semprini et al. 2000 [79]; Davis et al. 2002 [16])	Moderate phase partitioning coefficients, low molecular weight
Reaction					

(continued)

Table 7.4 (continued)

Tracer type	Injection phase	Application target parameters	Underlying processes	Exemplary compound classes	Most relevant tracer properties
<i>Tracer with chemical reaction (non-equilibrium tracers)</i>					
Kinetic interface-sensitive tracers (KIS tracer)	Non-aq.	Interfacial area and development with time	Hydrolysis at interface	Non-polar, hydrophobic esters (Schaffer et al. 2013 [76])	High log K_{ow} , reaction products anionic, suitable reaction rates
Thermo-sensitive tracers	aq.	Reservoir temperature, temperature gradients	Temperature-dependent hydrolysis	Polar, anionic esters (Nottebohm et al. 2012 [63])	Low log D , low pK_a , suitable reaction rates
Reactive esters for partitioning	aq.	Residual saturation of immiscible phases	In-situ generation of volume- sensitive partitioning tracers due to hydrolysis	Esters (reaction to alcoholic esters and alcohols) (Tomich et al. 1973 [86]; Myers et al. 2012 [57])	Water soluble, suitable hydrolysis rates of esters and partitioning coefficients of the reaction products
Biogeochemical reactive tracers	aq.	Transformation rates for certain domain, in-situ microbiological activity	Biological and/or chemical decay	Inorganic electron acceptors or donors (O_2 , NO_3^- , SO_4^{2-} , H_2) (Istok et al. 1997 [35]), low weight alcohols, benzoate, sugars (Rao et al. 2000 [70]), caffeine (Hillebrand et al. 2012 [33])	Labile (easily biodegradable) or reactive

aq. aqueous phase, non-aq. non-aqueous phase, gas. gaseous phase, log K_{ow} n-octanol/water distribution coefficient, log D pH-dependent n -octanol/water distribution coefficient of all species of ionizable organics, pK_a logarithmic acidity constant

principally be differentiated in conservative and non-conservative tracers. Conservative tracers that are physically and chemically inert and are classically applied for tracking connectivity and pathways for flow, for analyzing travel times, groundwater drift, and flow velocities, for determining recharge and discharge as well as for estimating hydromechanical reservoir properties such as dispersivity and porosity. In contrast, non-conservative tracers experience physico-chemical processes or chemical reactions during their transport. Therefore, they can provide information on physicochemical reservoir properties and the water chemistry (Schaffer 2013; Ptak et al. 2004; Divine and McDonnell 2005).

Table 7.4 gives an overview of the entire range of tracer types, their application and target parameters (e.g., porosity, dispersivity, interfacial area, residual saturation, etc.), the underlying process (e.g., adsorption on interface, hydrolysis), while providing examples of tracer compounds (e.g., perfluorocarbons, esters, etc.) and their most relevant properties (e.g., neutral molecules, water soluble, etc.).

7.3.2.2 Mathematical Models for Characterization of CO₂ Reservoirs

The mathematical models describing the fate of tracers and CO₂ injected into a geological formation are constructed on the equations of reactive single-phase and multi-phase flow and transport in porous and fractured media (Bear 1988). The single-phase formulations are mainly relevant for the site characterization stage while the multi-phase formulations apply more for the monitoring stage.

The mass balance equation for phase α in a multiphase flow porous media system can be expressed as (see also Chap. 3 for more elaborate development and definition of terms):

$$\frac{\partial(\phi\rho_\alpha S_\alpha)}{\partial t} + \nabla \cdot (\rho_\alpha v_\alpha) - \rho_\alpha q_\alpha = 0 \quad (7.3.7)$$

For accounting for dissolved component transport the mass balance equation is written:

$$\frac{\partial(\sum_\alpha \phi\rho_\alpha S_\alpha C_\alpha^k)}{\partial t} - \sum_\alpha \nabla \cdot \{\rho_\alpha v_\alpha C_\alpha^k + \phi\rho_\alpha D_\alpha^k \nabla C_\alpha^k\} - \sum_\alpha \rho_\alpha q_\alpha^k = 0 \quad (7.3.8)$$

where C_α^k is the concentration of the dissolved component k in the fluid-phase α . The mathematical models in Eqs. 7.3.7 and 7.3.8 can be reduced to a single-phase flow system by considering S_α equal to 1.

The source term q_α^k contains contributions from intra-phase α (where α can be wetting, w, or non-wetting, n) reactions and from partitioning between different phases. Generally, intra-phase reaction rates need to be multiplied by porosity and saturation to get the correct balance terms. Partitioning between phases can be at equilibrium or kinetic.

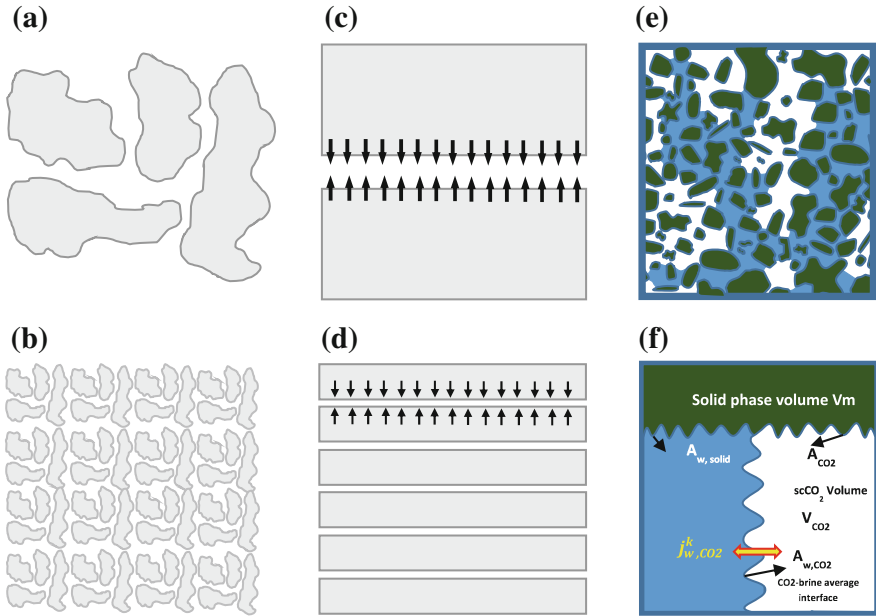


Fig. 7.13 Symbolic representations of fluid-rock (a–d) and fluid–fluid (e–f) interface-area density in porous media **a** a low specific contact surface area with the same bulk porosity as **b** high specific contact surface area; **c** fractured porous media: fracture-matrix fluid-rock interface area with low specific contact surface area and **d** high specific contact surface area, and the same bulk porosity; **e** wetting (blue)–non-wetting interface-area, **f** upscaled REV phase saturations, interface-area and exchange between phases (after Tatomin et al. 2015)

The Darcy velocity expressing the momentum conservation for fluid phase α is written:

$$v_\alpha = -\frac{k_\alpha}{\mu_\alpha} (\nabla p_\alpha - \rho_\alpha g) \tag{7.3.9}$$

The key parameter porosity ϕ is essentially a scaling factor in the storage term (time variable), while the size of fluid phase interface densities, $a_{\alpha\beta}$ (e.g., between CO_2 and brine) and fluid-solid interface densities, $a_{\alpha S}$ (Fig. 7.13) are coefficient factors in several of their reaction and solute exchange flux terms.

7.3.2.3 Target Parameters of Tracer Tests

The first of these parameters, ϕ is vital to any CCS project, in that it determines the storage capacity of the target formation and CO_2 plume spreading velocity under given injection rates. The importance of the second parameter $a_{\alpha\beta}$, the specific interfacial areas between fluid phases or between CO_2 and rock, may vary depending

on geological, hydrogeochemical and geotechnical details of the intended CCS site operation and fluid conditioning before injection. Fluid-rock interfacial area (density) $a_{\alpha S}$ (the specific interfacial area between fluid phase α and solid phase S) is a lumped averaged parameter, usually expressed in area per bulk reservoir volume, which relates to the effects of fracture spacing, length and aperture (Fig. 7.13). The mineral surface reactive area ($a_{\alpha S}$) is a key parameter for the mineral trapping (e.g., Xu et al. 2005; Luo et al. 2012). Term $a_{\alpha\beta}$ (the specific interfacial area between the two fluid phases α and β , e.g., water and gas) in turn, as determined in the characterization phase, can indicate the presence of a residual phase, such as oil or gas.

Apart from parameters ϕ , $a_{\alpha\beta}$ and $a_{\alpha S}$ the governing equations also contain, among their main variables, fluid phase saturations S_α as well as temperature T . These can also be treated as target parameters if, over the scale of a particular field experiment, they can be assumed to remain approximately constant.

Prominent examples aimed at determining the residual non-wetting phase saturation are the described in Tomich et al. (1973) for the residual oil saturation by means of single-well reactive-partitioning-tracer push-pull tests, and in Zhang et al. (2011) and Rasmusson et al. (2014) for the determination of CO_2 saturation using a combination of single-well hydraulic, thermal and partitioning-tracer push-pull tests. The determination of reservoir temperature by means of thermosensitive tracers is discussed in e.g. Nottebohm et al. (2012).

7.3.2.4 Tracer Tests for CO_2 Site Characterization

Historically, the tracers applied for site characterization have been well described in the field of hydrogeology (e.g., Leibundgut et al. 2009; Divine and McDonnell 2005). The use of liquid-phase conservative tracers, and the use of tracer diffusion, sorption or equilibrium-partitioning is based on well-established principles, models and application methods (Maloszewski and Zuber 1985, 1993; McCallum et al. 2005; Zuber and Motyka 1994; Carrera et al. 1998; Haggerty et al. 2001; Vulava et al. 2002), and shall not be further detailed here. Examples of tracer uses for site characterization is given in Table 7.5. Similarly, a synoptic view on the class of tracers termed “thermal tracers” used for reservoir thermal characterization is given in Table 7.6.

Generally, *inter-well tracer tests* are used to determine fluid residence time distributions (RTD). The statistical moments of RTDs provide important information about the reservoir (Ghargut et al. 2011), as follows:

1. The 0th-order RTD moment can tell something about reservoir boundaries.
2. The 1st-order RTD moment, or mean residence time (MRT) represents a measure of reservoir size (the reservoir volume that can be used for fluid storage).
3. The higher-order RTD moments provide information about reservoir heterogeneity. Traditionally, the 2nd-order moment is associated with flow-path dispersion (from hydrodynamic up to reservoir scale). From RTD analysis also a

Table 7.5 Examples of tracer uses for site characterization

Target parameter	Suitable method	Suitable tracer species	Limitations	Application examples
Transport-effective porosity	Inter-well tests; single-well inter-layer circulation	(Liquid-phase only) physico-chemically conservative, non-sorptive	Inter-well tracings cannot be conducted on a large scale at CCS candidate sites; tests remain limited to small-scale, pilot research projects; heterogeneity cannot be captured at reservoir scale	Deep saline aquifers in the N-German Sedimentary Basin (Horstberg, Gr. Schönebeck); geothermal: Kocabas (2005); oilfield: Kocabas and Maier (2013)
Fluid-rock interface area, fissure density	Inter-well tests; single-well tests	(Liquid-phase only) physico-chemically conservative, with contrast in sorption and/or diffusion; heat as a conservative fluid tracer	Parameter interplay; geological heterogeneity; geological uncertainty; parameter inversion requires the accurate knowledge of partitioning/sorption/diffusion coefficients independently of the field test	KTB pilot hole (heat and solute tracers); Bruchsal (attempted with heat as a tracer) (Behrens et al. 2014; Ghergut et al. 2013)
Relative saturation, fluid-fluid interface area (where applicable, in multi-phase systems)	Inter-well tests; single-well tests	Partitioning tracers		NAPL detection in the subsurface: Istok et al. (2002), Fagerlund (2007), LaForce et al. (2014)

Table 7.6 Summary of different meanings for thermal tracers and thermal characterization, single-well tests (SWT), inter-well tests (IWT)

Target information	Suitable method	Suitable tracer species	Limitations	Application examples
Site characterization: in situ measurement of thermal parameters (as an alternative to petrophysical laboratory techniques), for single-continuum descriptions	SWT	Heat as a conservative fluid tracer (fluid temperature signals)	May be disturbed by the presence of fractures/fissures	Kocabas (2005), Freifeld et al. (2008), Oberdorfer (2014)

(continued)

Table 7.6 (continued)

Target information	Suitable method	Suitable tracer species	Limitations	Application examples
Site characterization, cf. Table 7.1 (transport-effective porosity, dispersivity), for single-continuum descriptions	IWT SWT	Heat as a conservative fluid tracer (fluid temperature signals)	Pulse size limitation; not applicable on a large scale	Aquifer characterization: Anderson (2005), Read et al. (2013); theoretical studies of heat transport in porous media, esp. on the incongruence between heat dispersivity and solute dispersivity: Vandenbohede et al. (2009); thermal interference tests: Kocabas (2005), Oberdorfer et al. (2013)
Local characterization of single fractures; fissure aperture, fissure density in fissured media	SWT	Heat as a conservative fluid tracer (fluid temperature signals)	Requires continuous temperature recording downhole (ideally, DTS)	Pruess and Doughty (2010), Jung and Pruess (2012), Maier et al. (2012), Maier and Kocabas (2013)
Tracking thermal fronts in single-continuum media	IWT SWT	“Thermo-sensitive” tracers	pH and/or other non-predictable influences on tracer reaction rates	Nottebohm et al. (2012), Maier et al. (2014), Schaffer et al. (2015)
Tracking thermal fronts in fissured media	IWT	“Thermo-sensitive” tracers	Inversion methods are only developed for single-continuum descriptions; inversion not always unique for highly-heterogeneous, fissured/fractured media	Plummer et al. (2010), Juliusson and Horne (2010)

so-called flow-storage repartition (FSR) can be derived, which is sometimes interpreted as representing reservoir shape (cf. Shook and Forsmann 2005; Shook et al. 2004; Behrens et al. 2010).

Complementarily, *single-well tracer push-pull tests* are used to quantify processes other than advection-dispersion. Typically, they are used to quantify

exchange of some extensive quantity (mass, energy) between fluid and solid/fluid phases by processes like matrix diffusion or sorption/partitioning, the rate or amount of which depends on phase saturations and/or phase interface densities. Flow-field reversal during the ‘pull’ phase is supposed to largely compensate the effects of flow-path heterogeneity during the ‘push’ phase (excepting the hydrodynamic dispersion level), and, under certain conditions, to enhance the effects of tracer exchange processes at phase interfaces. In terms of determining different parameters in Eqs. 7.3.7–7.3.10 from different tracer tests, the following can be summarized:

- Porosity ϕ can only be measured reliably by means of inter-well conservative-tracer tests and it closely relates to tracer residence times.
- Rock-fluid and fluid-fluid interface area densities $a_{\alpha S}$, $a_{\alpha\beta}$ can be determined preferable by inter-well or alternatively by single-well tests using tracer pairs with contrasting properties in terms of: (a) *sorption*: is a process occurring at the fluid-rock interfaces, therefore, tracer testing using tracer components of contrasting sorption properties generate distinct breakthrough curves, implicitly offering a good sensitivity with respect to $a_{\alpha S}$, but rather poor sensitivity to S_{α} ; (b) *rock matrix diffusion* (for fluid-rock interfaces in fractured media): such tracer pair have a good sensitivity to $a_{\alpha S}$, but rather poor sensitivity to S_{α} ; (c) *‘intra-particle diffusion’* (for fluid-rock interfaces in unconsolidated porous media): these tracers have a good sensitivity with regard to S_{α} , but rather poor sensitivity to $a_{\alpha S}$; (d) *liquid-gas equilibrium partitioning* (for liquid-gas interfaces): this pair of tracers have good sensitivity to S_{α} , but rather poor sensitivity to $a_{\alpha\beta}$; (e) *liquid-gas interface reactivity*, with dichotomic partitioning of reaction products (for liquid-gas interfaces), as proposed by Schaffer et al. (2013): these tracers have a good sensitivity to both $a_{\alpha\beta}$ and S_{α} .

Use of tracers for CO₂ monitoring is discussed in Chap. 8 and for the specific use of characterizing site’s capacity for CO₂ residual and dissolution trapping in Sect. 7.4.

7.3.3 Characterization of the Thermal Properties

Jacob Bensabat

In the context of CO₂ storage, it is important to be able to predict pressure and temperature conditions of the injected CO₂ along the CO₂ injection tubing and at the well bottom. This requires the ability to simulate the injection of the CO₂ in the borehole, from the wellhead to the well bottom. The temperature and pressure of the CO₂ at the well bottom will depend (i) on the pressure and temperature conditions of the CO₂ at the wellhead, which are determined by the operator of the injection, (ii) on the pressure losses along the injection tube and (iii) the heat transfer between the injected CO₂ and its surrounding environment. As the temperature of the injected CO₂ will be different from the temperature of its environment along the

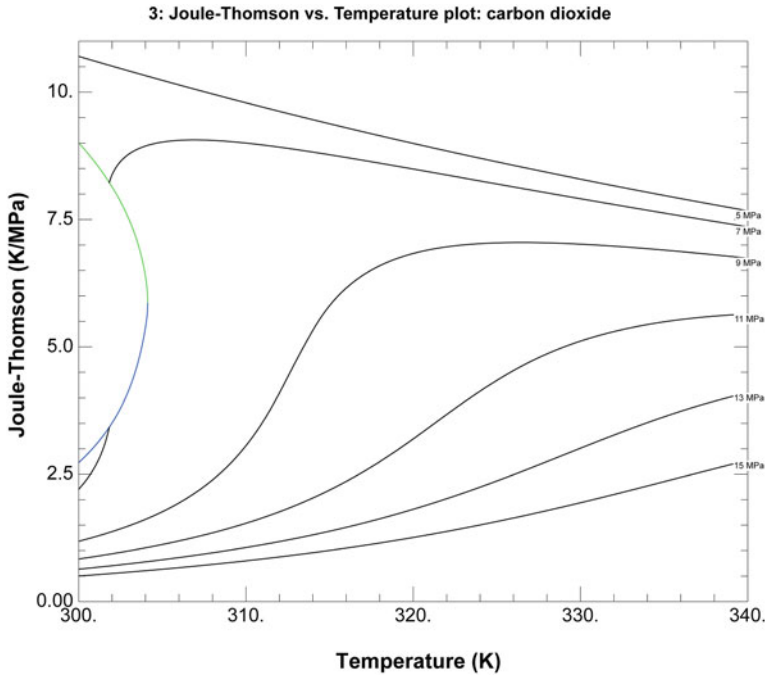


Fig. 7.14 Joule–Thomson coefficient for CO₂ (generated with REFPROP 9; NIST 2010)

borehole, there will be heat exchange, which depends on the configuration of the well and on the thermal properties of the geological materials surrounding the well.

Pressure losses are calculated from the CO₂ properties and from the characteristics of the injection tube. For small scale CO₂ injection experiments, these can be regarded as of secondary importance due to the very low viscosity of the CO₂ and to the generally small injection flow rates (less than 20 tons/h). This process is governed by the Joule–Thomson coefficient, which for CO₂ is presented in Fig. 7.14.

Thermal exchange between the injected CO₂ and its surrounding environment will depend on the well configuration, on the casing and cement properties and on the thermal properties of the surrounding formation and its temperature. This process of heat transfer can be defined as radial heat transfer and the rate of heat flow per unit length of well can be expressed following Hasan and Kabir (2002):

$$Q = -2\pi r_o U_o (T_f - T) \quad (7.3.10)$$

where U_o is the overall heat transfer coefficient, between the CO₂ inside the injection tube and the formation. r_o denotes the radial distance between the injection tube and the formation, T and T_f are the wellbore and the formation temperatures. Simulations of the CO₂ injection in the wellbore indicate that the temperature of the

CO₂ at the well bottom is highly dependent on the heat transfer by radiation between the flowing CO₂ and its environment, described by the heat transfer coefficient.

There are many possibilities of well configuration and as an example we shall consider a well configuration similar to the wells drilled in the frame of the MUSTANG project at Heletz site in Israel (for details see Niemi et al. 2016).

These type of wells are divided in three vertical sections:

1. **The upper section** between ground surface and a depth of ~ 300 m. This section includes the geological formation, cement, the outer casing (13^{5/8} in. diameter), cement, the middle casing (9^{5/8} in.), cement, inner casing (7 in. diameter), fluid, and the injection tube (2^{3/8} in. diameter).
2. **The middle section** between the depth of 300 m and a depth of 1200 m. This section includes the geological formation, cement, a 9^{5/8} in. diameter casing, cement, the 7 in. diameter casing, fluid and the 2^{3/8} in. diameter injection tube.
3. **The lower section** between the depth of 1200 m and to the well bottom at 1650 m. This section includes the formation, cement, the 7 in. casing, fluid and the injection tube.

There may be many alternative well configurations than the above one. The overall heat transfer coefficient represents the resistance to heat flow from the tubing to the formation and convective heat flow in the annulus (which may possibly be filled with water in the lower part or air in the upper part). Without loss of generality, we present an expression for this coefficient for lower, and simpler, part of the casing. Developing an expression for the other parts is straightforward.

$$\frac{1}{U_o} = \frac{r_{to}}{r_{ti}h_{to}} + r_{to} \left[\frac{\ln\left(\frac{r_{to}}{r_{ti}}\right)}{\lambda_{tubing}} + \frac{\ln\left(\frac{r_{to}}{r_{ci}}\right)}{\lambda_{annulus}} + \frac{\ln\left(\frac{r_{co}}{r_{ci}}\right)}{\lambda_{ca\ sin\ g}} + \frac{\ln\left(\frac{r_{wb}}{r_{ca}}\right)}{\lambda_{cement}} + \frac{\ln\left(\frac{r_{f\infty}}{r_{wb}}\right)}{\lambda_{formation}} \right] \quad (7.3.11)$$

where r_{ti} and r_{to} denote the inner and outer radii of the injection tube, r_{ci} and r_{co} denote the inner and outer diameters of the casing, r_{wb} is the wellbore diameter, $r_{f\infty}$ is a radial distance in the formation at which the field temperature is not affected by the injection and r_{wb} is the wellbore radius. λ_{tubing} , $\lambda_{annulus}$, $\lambda_{ca\ sin\ g}$, λ_{cement} and $\lambda_{formation}$ denote the thermal conductivities of the tubing, the fluid filling the annulus, the casing, the cement and the formation, respectively. h_{to} denotes the rate of heat transfer between the flowing CO₂ and the inside of the injection tubing wall. We assume that the radial heat transfer adjusts instantaneously (quasi-steady state conditions) and we neglect convective processes in the annulus. These assumptions allow us to determine a lumped coefficient, responsible for the heat exchange between the formation and the injection tubing. All of the parameters but two in above formula can be determined. These are thermal conductivity of the formation $\lambda_{formation}$ and the thermal radius of influence of the well, $r_{f\infty}$, or the radial distance from the well at which no thermal effect resulting from the injection of the CO₂ is felt.

The key missing information above is therefore the thermal conductivity of the various formation layers. We present below an experimental sequence aimed at determining these data in situ and suggest the following procedure:

1. If logs are available, so it is possible to have a lithological description of the well section and to construct a discrete division of the well lithological profile with homogeneous geological properties (of homogeneous thermal conductivity for each unit).
2. Measure the temperature along the well, from well head to well bottom. Depending on the well completion, this could be performed in two ways: 1) using distributed temperature sensing (DTS) if that is included in the well completion (see Sect. 8.4) using a temperature probe and attached to a winch for vertical up-and-down scanning of the borehole.
3. Inject cold water, or water with a substantially lower temperature than the one along the well in the formation. Use formation water previously abstracted, in order to prevent any unwanted chemical reaction between formation water and the injected one (such as swelling of clay particles, oxidation and others).
4. Wait until static conditions have been reached, and there is no flow in the tubing.
5. Measure the temperature recovery in the well until the full return to the initial temperature.
6. If there is information available allowing splitting of the well lithology into a series of quasi-homogeneous sections, start from this division and further refine it by analyzing the rate of the thermal recovery along the well. Areas of high thermal conductivity would recover faster than other areas of lower thermal conductivity. If there is no lithological information, use only the temperature time series.
7. Since there is no flow in the well, the temperature recovery in the tubing can be expressed by the following heat balance equation.

$$\frac{\partial T}{\partial t} = \frac{\lambda_w}{\rho_w C_{pw}} \frac{\partial^2 T}{\partial z^2} + U_0(z)(T(z) - T_f(z)), \quad z \in [z_b, z_t] \quad (7.3.12)$$

$$U(z) \equiv \sum_{i=1}^{N-1} (H_i(z) - H_{i+1}(z)) U_{oi} \quad (7.3.13)$$

The heat balance equation above has known initial and boundary conditions of temperature, i.e.

$$T(z_t) = T_t \quad (7.3.14)$$

$$T(z_b) = T_b \quad (7.3.15)$$

$$T(t = 0, z) = T_0(z) \quad (7.3.16)$$

where $H_i(z)$ is a Heaviside type function, defined as:

$$H_i(z) = \begin{cases} 0 & \text{if } z < z_i \\ 1 & \text{if } z \geq z_i \end{cases}. \quad (7.3.17)$$

N is the number of vertical lithological partitions. $T(z)$ is the temperature of the water in the tubing and $T_f(z)$ is the temperature in the formation, which is equal to the initial temperature profile. The heat balance equation (7.3.12) together with the initial and boundary conditions (7.3.14–7.3.16) can be solved analytically or numerically.

In the case of the thermal test the overall heat transfer coefficient is simpler, as there is no flow in the tubing and reduces to:

$$\frac{1}{U_o} = r_{to} \left[\frac{\ln\left(\frac{r_{to}}{r_{ti}}\right)}{\lambda_{tubing}} + \frac{\ln\left(\frac{r_{to}}{r_{el}}\right)}{\lambda_{annulus}} + \frac{\ln\left(\frac{r_{co}}{r_{el}}\right)}{\lambda_{ca \sin g}} + \frac{\ln\left(\frac{r_{wb}}{r_{co}}\right)}{\lambda_{cement}} + \frac{\ln\left(\frac{r_{\infty}}{r_{wb}}\right)}{\lambda_{formation}} \right]. \quad (7.3.18)$$

The determination of the parameter U_o for each vertical partition can be obtained via an inverse procedure, i.e., minimizing the least squares of the errors between measured and simulated temperature over a range of time intervals and vertical sections.

We first divide the time interval that is required for the tubing to return to the initial temperature distribution in N_t equally spaced intervals of size Δt .

The identification procedure can be formally expressed as the following least-squares problem:

$$F(U_o) = \min \sum_{i=1}^{i=N_t} \sum_{p=1}^{p=N} [T(i, p) - T_s(U_o(p), i, p)]^2 \quad (7.3.19)$$

where $T(i, p)$ is the measured temperature, characteristic of the vertical section p at time $t_0 + i\Delta t$. $T_s(U_o(p), i, p)$ is the simulated temperature, which depends on the value of the overall heat transfer coefficient at the same time and vertical section.

7.4 CO₂ Injection Tests as a Characterization Method

Fritjof Fagerlund and Auli Niemi

CO₂ injections can be used to obtain knowledge about formation parameters which are directly related to the behaviour and fate of the injected CO₂. These include parameters which govern (i) the two-phase flow of a CO₂-rich and an aqueous phase, (ii) parameters governing CO₂ trapping in the formation and (iii) interactions between CO₂ and formation fluids and rock. Carefully monitored CO₂ injections have been performed in research projects including sites such as Frio (e.g. Hovorka et al. 2006), Otway (e.g. Paterson et al. 2013a, b, 2014) and Ketzin (e.g. Würdemann et al. 2010) and are underway at sites such as Heletz, Israel (Niemi et al. 2016) and Hontomin. Here the objectives typically have been related to gaining fundamental knowledge about geological CO₂ storage and the fate of the injected CO₂, or the development of field methods. Small-scale CO₂ injections can be useful both at pilot test sites and at sites under consideration for large-scale geological storage, to obtain better knowledge about site-specific properties related to site performance, such as field-scale CO₂ trapping or effective storage capacity.

Trapping of injected CO₂ by processes additional to the accumulation under a structural trap improves the storage security and is essential at many potential storage sites. Due to e.g. heterogeneity at different scales and the resulting preferential flow paths, these processes may differ in both magnitude and timing at the field scale as compared to laboratory investigations on rock cores or theoretical analyses. Field investigations concerning the trapping processes are therefore essential to understand the effective in situ trapping. In following sections, we will present examples field tests designed to study residual phase CO₂ trapping and dissolution trapping in situ. First the field-scale nature of the trapping processes and available measurements will briefly be discussed.

7.4.1 *Field-Scale Residual and Dissolution Trapping*

Residual phase trapping is a pore-scale process which occurs as small blobs and ganglia of the free-phase CO₂ (the non-wetting phase) are snapped off and become immobilized. However, due to heterogeneity in capillary properties of the medium, the non-wetting phase is also trapped at capillary barriers, thus forming small-scale structural traps.

At the field scale, the total residual phase trapping depends on (i) the amount of residual trapping that occurs per unit volume swept by the free-phase CO₂ (including both the pore-scale trapping and trapping at capillary barriers), and (ii) the sweep efficiency of the free-phase CO₂ plume (Hesse et al. 2009). Much uncertainty remains in quantifying both these parameters in relevant CO₂ storage formations. For poor sweep efficiencies when the CO₂ moves as a thin pancake under the cap rock ceiling, the CO₂ can move very large distances before it becomes immobilized, thereby increasing the risk of reaching a spill point (Hesse et al. 2009).

The pore-scale residual trapping in the aquifer volume swept the free-phase CO₂ depends on the local maximum CO₂ saturation (S_{gmax}) and the local initial gas saturation at the start of imbibition (S_{gi}), and such a dependence can be described by a trapping model (Land 1968). For a comparison of the effect of using different trapping models on CO₂ trapping, the reader is referred to Rasmusson et al. (2016). Thus, locally, the final residual saturation S_{grf} after imbibition of the aqueous phase is a function of the maximum possible residual saturation, S_{grmax} , and the initial CO₂ saturation at the start of imbibition, S_{gi} . S_{grmax} is a material property which influences the capacity for residual trapping in a formation. Characterization methods aimed at determining this property have therefore been developed for e.g. the CO₂ injection experiments at Otway (Zhang et al. 2011; Paterson et al. 2013a, b, 2014; LaForce et al. 2014), and the planned experiments at Heletz (Rasmusson et al. 2014).

Heterogeneity is also critical for the residual trapping of CO₂ (e.g. Green et al. 2009; Flett et al. 2007; Hovorka et al. 2004) as it can strongly affect the sweep efficiency and thereby the saturation history. However, the net effect of heterogeneity on residual trapping appears to be dependent both on the nature of the heterogeneities and the general direction of movement of the CO₂ plume, as it can be different for vertical and horizontal migration (see e.g. Tian et al. 2016). Furthermore, it has been suggested that the strategy for CO₂ injection has a large impact on the sweep efficiency and subsequent residual trapping (e.g. Qi et al. 2009, Rasmusson et al. 2016). Qi et al. (2009) suggested that water should be co-injected with the CO₂ at a ratio which produces such mobility ratio between the two fluids that the sweep is maximized.

Dissolution of CO₂ to the aqueous phase can improve storage security as heavier CO₂-rich water sinks and thereby produces a vertical convective mixing which further enhances the dissolution process (e.g. Ennis-King and Paterson 2005; Riaz et al. 2006). Enhanced CO₂ dissolution by convective mixing is, however, a process that has mainly been studied using theoretical analyses and numerical modeling; e.g. Ennis-King and Paterson (2005), Riaz et al. (2006), Pau et al. (2010), and in analogous laboratory experiments (e.g. Kneafsey and Pruess 2010; Neufeld et al. 2010). There is therefore a strong need to measure and demonstrate this process in the field and characterize the key field-scale properties influencing the long-term significance of CO₂ dissolution at given storage sites. While long term experiments are needed particularly to observe convective mixing, much can be learned about the dissolution process and the interaction between the aqueous and CO₂-rich phases including the immobile (residual) water and CO₂ (Paterson et al. 2013a, b; Fagerlund et al. 2013a).

7.4.2 Field Measurements Related to Two-Phase Flow and Trapping

Measurements of fluid saturations as well as the parameters affecting two-phase flow and trapping of CO₂ are highly challenging at the depth of typical storage formations (>800 m). Measurements are restricted to inside or in the direct vicinity

of boreholes, which are typically scarce due to the difficulties and costs associated with drilling at such depths. Surface geophysical measurements can generally not be used to visualize the two-phase flow and trapping at the typical depths to the required detail. To characterize the related aquifer properties one has to rely on the measurements available in deep wells. A strategy to characterize CO₂ trapping has therefore been to combine the information from several types of measurements which are influenced by the CO₂ trapping and to use inverse modeling to infer the trapping properties (Zhang et al. 2011).

In a characterization experiment involving CO₂ injection, a test sequence can be employed where the same measurements and tests are repeated both without CO₂ in the formation (before CO₂ injection) and with CO₂ in the formation (after CO₂ injection) (e.g. Paterson et al. 2013a, b). Measurements which can be included in such test sequence include:

Pressure or hydraulic test: Water is injected at a given rate (or pressure) and the pressure (or flow rate) in the injection well and other available wells is monitored using pressure sensors in the wells. The pressure signal is affected by the relative permeability to the aqueous phase, which is a function of fluid saturation. When performed with CO₂ at residual saturation the test gives information about the residually trapped saturation. To avoid dissolution and a change in saturation during the test, water saturated with dissolved CO₂ can be injected when creating the residually trapped zone (Zhang et al. 2011).

Thermal test: The concept of a thermal test for CO₂ saturation characterization has been described by Freifeld et al. (2008), and such test was applied at Ketzin (Giese et al. 2009) and Otway (Paterson et al. 2013a, b). The formation is heated from a borehole using a resistance heater and subsequently allowed to cool, while the temperature is measured using a fibre-optic distributed temperature sensor (DTS—more information given in Sect. 8.4 Well instrumentation). The dissipation of heat and thus the temperature signal is influenced by the effective thermal conductivity, which, in turn, is a function of fluid saturation since supercritical CO₂ has significantly smaller thermal diffusivity and specific heat capacity as compared to brine at typical reservoir pressures and temperatures. The sensitivity of this test is related to porosity since for a lower porosity the influence of the fluid in the pore space becomes smaller. A thermal test can penetrate in the order of 1–2 m into the formation depending on the applied heat and the rock properties (Zhang et al. 2011).

Pulsed Neutron Capture Tool (RST): This well-logging technique is sensitive to hydrogen index and thus also to the saturation distribution of CO₂ and brine near the borehole. It was successfully used to measure CO₂ saturation in the direct vicinity of boreholes at Frio (Doughty et al. 2008) and Otway (Paterson et al. 2013a, b). A limitation of the method is however that the penetration depth is only in the order of 0.20 m.

Tracers: Tracers are potentially very useful for the characterization of deep CO₂-brine systems, since the tracers can bring out information from aquifer volumes which are difficult to access with any other technique. However, much testing remains to be done employing tracers and interpreting the tracer response in these systems. Partitioning tracers, which are injected with the aqueous phase and

retarded due to partitioning into an immobile fluid phase such as residual CO_2 , provide information about the amount of immobile fluid present. This technique has been used to detect non-aqueous phase liquid (NAPL) pollutants (e.g. Istok et al. 2002) and also in single-well push-pull tests to infer residual CO_2 saturation (Paterson et al. 2013a, b). Paterson et al. (2013a, b) used the noble gas tracers Kr and He which were injected with water and produced different breakthrough signals as the water was pulled back to the well due to the different partitioning behaviour (Henry's constants) of the two tracers. The differences in partitioning and comparison to the case of no partitioning (no immobile fluid phase present or a conservative tracer) were used to calculate the residual CO_2 saturation. Reactive partitioning tracers which form daughter products in connection with the partitioning have been used to measure residual oil saturation (Tomich et al. 1973). In the push-pull tests at Otway (Paterson et al. 2013a, b) a similar reactive tracer technique was also employed, but with organic tracers more adapted to the partitioning between brine and supercritical CO_2 , as described in more detail by Myers et al. (2012). Furthermore, new reactive tracers—kinetic interface sensitive (KIS) tracers—aimed at quantifying the interface between two immiscible phases are being developed (Schaffer et al. 2013) and can also be used in the characterization of a CO_2 -brine system. Tracer techniques can be employed in both single-well push-pull tests and two-well (or multi-well) inter-well tests. Partitioning inter-well tracer tests (PITTs) have been used for measurement of residual oil saturation (e.g. Du and Guan 2005; Tang 2005) with applications in petroleum industry, and have also been used for contamination characterization measuring NAPL saturations (e.g. Nelson et al. 1999; Jin et al. 1995; Mariner et al. 1999). PITTs are also planned at the Heletz site to measure residual CO_2 saturation in a dipole test (Fagerlund et al. 2013a). In these dipole field tests, tracers are also planned to be used to measure the (short-term) dissolution of mobile and immobile (residual) CO_2 . As described in more detail by Fagerlund et al. (2013a), the idea is that a tracer with extreme affinity for the CO_2 phase is injected with the CO_2 . As the CO_2 dissolves into the formation brine, this tracer (which has negligible aqueous solubility) is enriched in the CO_2 phase. Thus, when the injected CO_2 breaks through to the withdrawal well, it carries information about the amount of mobile supercritical CO_2 which has been dissolved during its migration between the two wells. The dissolution of immobile CO_2 can further be quantified by measuring the CO_2 concentration in the extracted brine. Numerical modeling indicates that tracer techniques potentially can be used to identify the point in time when conditions of residually trapped CO_2 have been established, which can be critical in characterization experiments aimed at quantifying the residual CO_2 trapping. This indicator tracer method has been outlined to more detail by Rasmusson et al. (2014).

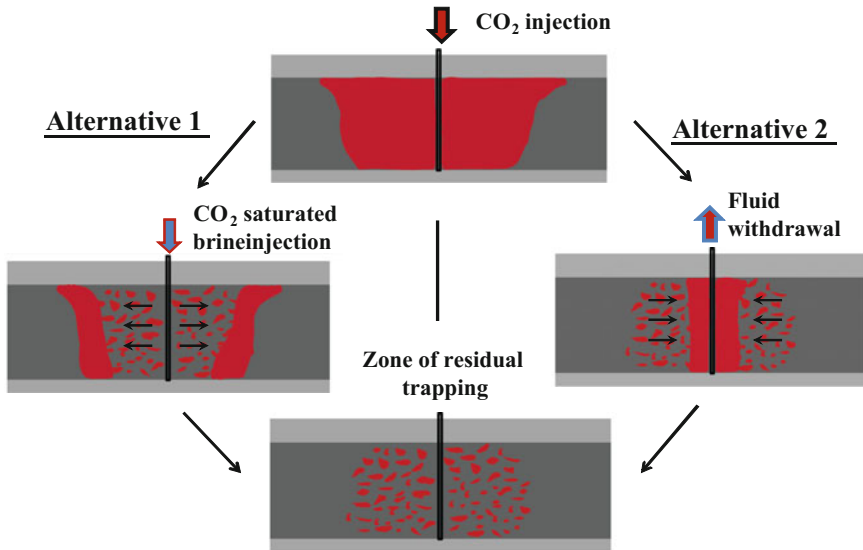


Fig. 7.15 Alternatives for creating a zone of residually trapped CO₂ in a push–pull field test

7.4.3 *Single-Well Push–Pull Test for Quantification of Residual Trapping*

This section describes the basic concept of a push–pull field test to quantify residual trapping of CO₂ and is mainly based on the test performed at Otway (Paterson et al. 2013a, b; Zhang et al. 2011) and the planned experiments at Heletz (Rasmusson et al. 2014).

Before residual trapping can be quantified, a zone of residually trapped CO₂ must be created in the storage formation. The creation of such zone and verification that the CO₂ phase has become immobile by residual trapping may not be trivial. Two alternatives have been proposed. As illustrated in Fig. 7.15, the first alternative is to inject CO₂ saturated water following the injection of free-phase CO₂. The CO₂ phase is pushed away by the injected brine, but does not dissolve because the brine is already saturated with CO₂. This option was chosen in the field tests at Otway (Paterson et al. 2013a, b). A technical challenge, as experienced in these experiments, can be the mixing of CO₂ into the brine injection and achieving brine just saturated with CO₂ (but not over saturated) at the reservoir pressure and temperature. Following injection of CO₂, a second alternative for creation of the zone of residual trapping (Alternative 2 in Fig. 7.15) is to withdraw formation fluids until the remaining CO₂ phase is immobilized by residual trapping. This method has the drawback that it may be difficult to know when the free-phase CO₂ has become immobile, and thus, to know when to stop withdrawing fluids (Zhang et al. 2011). Too much withdrawal will result in dissolution of the residually trapped CO₂ and

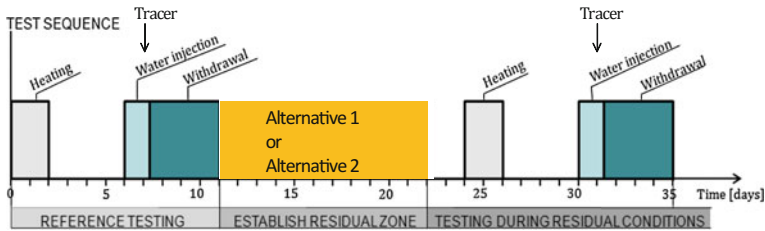


Fig. 7.16 Schematic example of a test sequence for a push-pull field test to characterize residual CO_2 trapping (Rasmusson et al. 2014)

may bias the quantification of residual trapping. A possible solution to this issue has been proposed by Rasmusson et al. (2014) who suggest the use of a conservative indicator tracer which according to modeling results can indicate the time when residual trapping has been achieved.

Both alternatives for creating the zone of residual trapping may be affected by buoyancy flow of the CO_2 phase and geological heterogeneity leading to preferential flow patterns in the formation. Particularly for high permeability, buoyancy flow towards the storage formation ceiling can be significant compared to the pressure driven flow through the well. Thereby a “pancake” of higher saturation free-phase CO_2 will form under the formation ceiling, under the caprock, the saturation distribution becomes uneven in the vertical direction and residual trapping occurs at later times in the top part which is refilled from below, and where the flow along the ceiling is slow.

Geological heterogeneity can influence the flow of both the CO_2 and brine phases. The CO_2 phase may preferentially move in high-permeability, low-entry-pressure channels or formation volumes, thereby affecting the sweep efficiency of the free-phase CO_2 and also the effective amount of residual trapping over the sampled volume. Potential bias in the residual trapping quantification both in terms of effects on sweep efficiency and fluid saturation history must therefore be considered in the test evaluation.

The strategy to quantify the residual trapping in the Otway field test (Paterson et al. 2013a, b; Zhang et al. 2011) was to include reference tests before the creation of the zone of residual saturation so that the same tests and measurements could be performed both with and without residually trapped CO_2 present in the formation. This method reduces some effects of heterogeneity on the test results since the same heterogeneity is seen by the measurements before and after introducing the CO_2 . A schematic example of such test sequence is shown in Fig. 7.16, which includes (1) reference tests without CO_2 in the formation, (2) the creation of the zone of residual trapping, and (3) characterization tests with residual CO_2 present. Other tests than the hydraulic, thermal and tracer tests shown here (such as RST logging or cross-hole geophysical measurements) can also be added to the test sequence.

The responses in hydraulic, thermal and tracer tests with and without residual CO_2 in the formation all carry information about the residual trapping.

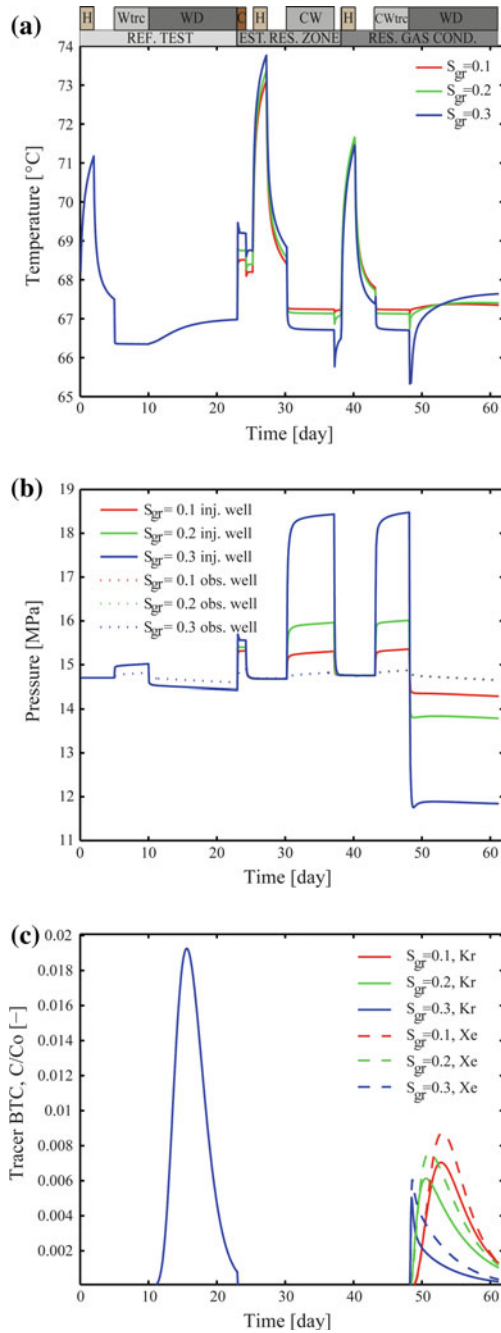


Fig. 7.17 Simulated response for different values of residual trapping (S_{gr}) in **a** temperature, **b** pressure (in both the injection well and an additional observation well) and **c** tracer BTCs for the noble gases Kr and Xe. From Rasmusson et al. (2014)

A process-based model can be used to jointly interpret the information of different measurements and estimate the residual trapping under uncertainty in different model parameters using inverse modeling techniques.

Examples of modeled responses in temperature, pressure and tracer breakthrough curves for different values of residual CO_2 trapping are shown in Fig. 7.17. This example comes from the design modeling for push–pull field tests at the Heletz site (Rasmussen et al. 2014), which is based on the field tests and modeling strategy developed for the Otway site (Zhang et al. 2011), and roughly follows the schematic test sequence presented in Fig. 7.16. As can be seen in Fig. 7.17, the responses in the measurements differ for different values of residual trapping (S_{gr}), however the sensitivities to S_{gr} vary in magnitude and change with time. A clear pressure increase which is sensitive to S_{gr} is for example seen when CO_2 saturated water is injected to create the zone of residual trapping roughly between 31 and 37 days (Fig. 7.17b) as well as in the following hydraulic test (water injection) during the characterization phase.

A prerequisite to successful estimation of the residual trapping is that the sensitivities to S_{gr} of the available measurements are large enough. However, because the measurement responses also depend on other uncertain parameters, the correlations between S_{gr} and these parameters need to be investigated and reduced. A systematic sensitivity and uncertainty analysis is essential with this approach and can also identify additional data needs to constrain the estimates of trapping. As shown by Zhang et al. (2011), combining several data sets and different data types reduces estimation uncertainties and improves the estimates of S_{gr} .

7.4.4 Two-Well Test for Quantification of Residual Trapping and Dissolution

This section describes the concept of a two-well field test to quantify residual trapping of CO_2 and dissolution. It is mainly based on simulation studies by Fagerlund et al. (2013a, b) aimed at exploring two-well field methods planned for the Heletz field site to characterize CO_2 residual trapping and dissolution under influence of geological heterogeneity.

In single-well push–pull experiments, fluids are pushed out and pulled back through the same flow channels, which can reduce the influence of geological heterogeneity. In inter-well tests, the flow and transport is affected by the heterogeneity between the wells and typically the transport also goes through a larger aquifer volume than in a push–pull test. Combining single-well push–pull tests with inter-well tests can therefore provide information about the effect of geological heterogeneity on the flow and trapping processes of injected CO_2 . Both passive and actively pumping observation wells can be considered for monitoring of the CO_2 migration from the injection well. In this example we consider an active withdrawal well. This option has the advantages that (i) the flow field to some extent can be

controlled by withdrawal of fluids, (ii) a zone of residual trapping between the wells can be established, and (iii) formation fluids and tracers can be measured as they are withdrawn from the observation well. The withdrawal of both formation brine and free-phase CO_2 which has migrated through the formation allows analysis of fluid compositions carrying information about the interphase mass transfer in the formation. Furthermore, tracers in both the aqueous and CO_2 -rich phases can be analysed.

This example (based on Fagerlund et al. 2013a, b) will be limited to (i) a hydraulic test aimed at measuring residual trapping of CO_2 in the region between the two wells, and (ii) a tracer in the CO_2 -rich phase which together with analyses of the withdrawn fluid compositions can be used for quantification of effective rates of CO_2 dissolution in the formation. Other tests as described above can, of course, be added to the test sequence, adding information and reducing uncertainty in the estimates as described above. The hydraulic test is repeated before and after CO_2 injection and the difference in the pressure response can thus be used to infer the reduction in aqueous phase permeability due to presence of residually trapped CO_2 .

The tracer technique involves injection of a tracer with very small aqueous solubility with the CO_2 . Thereby, as CO_2 dissolves into formation brine, the tracer is enriched and if tracer dissolution is negligible, the enrichment is directly proportional to the CO_2 dissolution. When free-phase CO_2 arrives at the withdrawal well, the tracer concentration in the CO_2 rich phase carries information about the amount of dissolution of mobile free-phase CO_2 which has occurred during its flow between the wells.

A schematic test sequence for the two-well test is shown in Fig. 7.18. The upper half of the figure shows the injection well activity and the lower part shows the withdrawal (abstraction) well. A reference hydraulic test is included before the injection of CO_2 , and the hydraulic test is then repeated at the stage when most of the free-phase (supercritical—sc) CO_2 in the formation has been immobilized by residual trapping. To draw fluids and tracers, and to control the flow field,

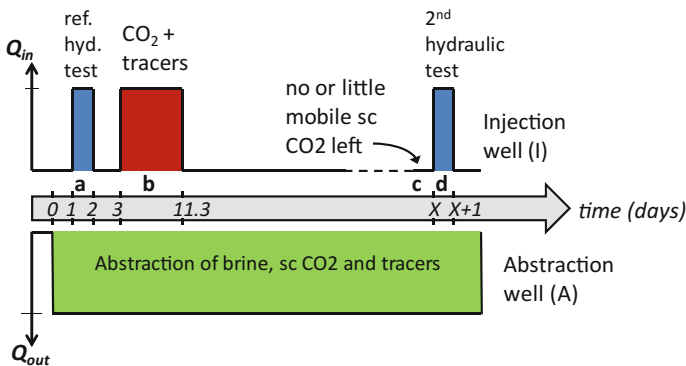


Fig. 7.18 Proposed two-well injection-withdrawal sequence. Time zero is the start of the reference hydraulic test. From Fagerlund et al. (2013a)

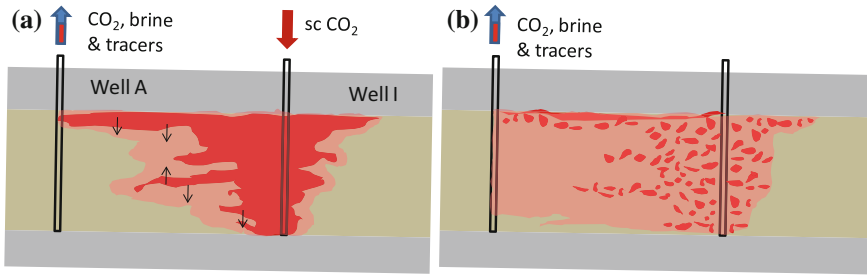
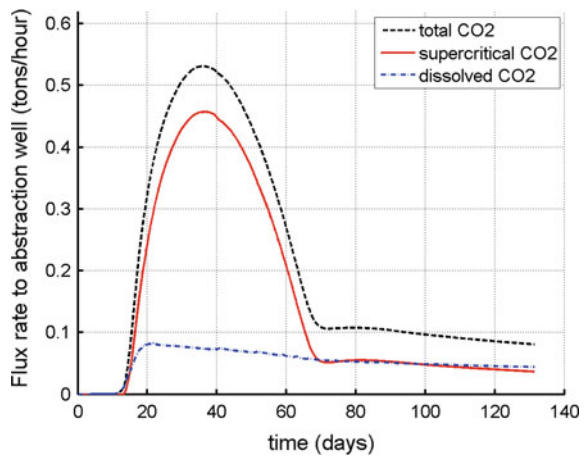


Fig. 7.19 Two-well CO₂ injection experiment at free-phase CO₂ breakthrough to the withdrawal well (a) and at residual state of free-phase CO₂ (b). From Fagerlund et al. (2013a)

Fig. 7.20 Flux of CO₂ to the withdrawal well. From Fagerlund et al. (2013a)



continuous withdrawal from the second well is maintained throughout the test sequence. Residual trapping and dissolution occurs as the CO₂ migrates through the formation between the two wells, and after a period of fluid withdrawal most of the free-phase CO₂ will be residually trapped. The concept is illustrated schematically in Fig. 7.19. The aim of this two well test is to quantify the residual trapping that occurs under influence of geological heterogeneity and potential preferential flow paths that exist at the field site.

To identify the conditions of residual trapping in the formation, the point in time when very little mobile free-phase CO₂ remains needs to be identified, and this time can of course be different dependent on the formation properties and test configuration. Design simulations for the planned experiments at Heletz indicate that the conditions of residual trapping can be identified by measuring the flux of CO₂ to the withdrawal well. An example from this is shown in Fig. 7.19, where a clear change in the rate of supercritical (and total) CO₂ extraction can be seen at approximately 70 days after start of the test sequence. This change in flux rate corresponds to achieving the state of residual trapping as illustrated schematically in Fig. 7.20.

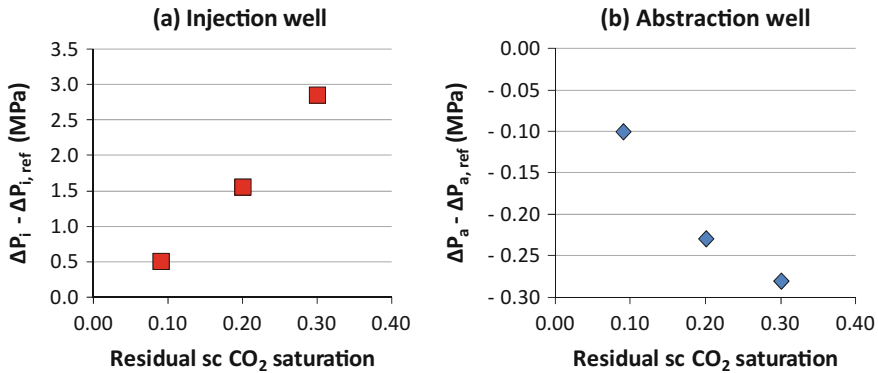


Fig. 7.21 **a** Simulated difference between the maximum pressure during the reference hydraulic test and the hydraulic test with residually trapped CO₂ in the injection well for different amounts of residual trapping. **b** Similarly, difference in minimum pressures in the abstraction well. From Fagerlund et al. (2013a)

The inter-well distance chosen for the test together with the rate of pumping has a large effect on the time required to reach a state of residual trapping (Fagerlund et al. 2013a).

Similar to the push–pull experiments discussed above, simulations of the two-well experiment test sequence have shown that the pressure response in the hydraulic test is highly sensitive to the residual trapping as a result of reduced permeability to the aqueous phase in the presence of trapped CO₂. An example is given in Fig. 7.21 which shows the simulated difference in the maximum pressure during the reference hydraulic test and the hydraulic test at residual trapping conditions in the injection well (Fig. 7.21a), and similarly, the difference between minimum pressures in the withdrawal (abstraction) well (from Fagerlund et al. 2013a). While the total pressure change depends also on the permeability (not shown here), the sensitivity to different amounts of residual trapping is clear both in the injection and withdrawal wells. Both wells can thus contribute to the estimation of the residual trapping between the wells.

Measurement of the concentration of CO₂ in the withdrawn brine allows analysis of the amount of dissolution that occurs in the formation. For the test configuration with active withdrawal of fluids Fagerlund et al. (2013a) found a strong correlation between the rate of CO₂ abstraction and the effective rate of CO₂ dissolution in the formation. As shown in Fig. 7.22, the correlation was linear for a wide range of different simulation scenarios producing different groundwater flow fields and effective total dissolution in the formation. From these modeling studies it was therefore concluded that for the stable flow field maintained using continuous withdrawal of fluids, the total rate of CO₂ dissolution in the formation could be inferred from measurements of abstracted CO₂.

Simulations of the negligible-solubility tracer (NST) test have shown that the enrichment of the tracer in the abstracted free-phase CO₂ is directly correlated to the

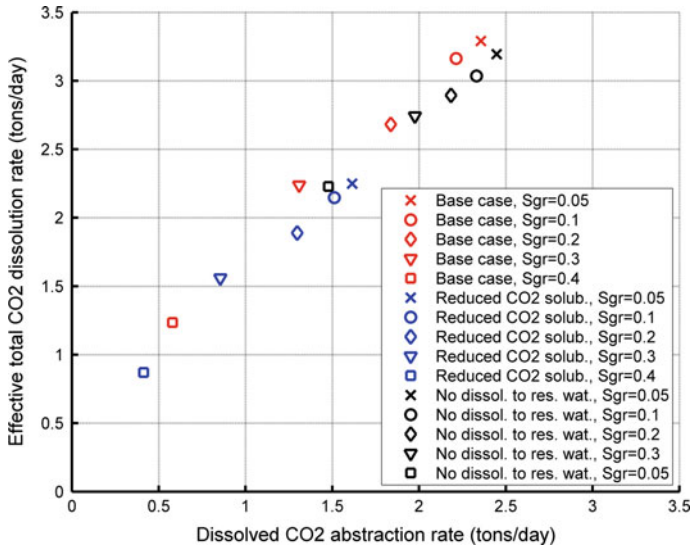


Fig. 7.22 Relationship between rate of CO₂ abstraction and the effective total rate of dissolution in the formation for a range of simulation scenarios producing different flow fields and dissolution rates. From Fagerlund et al. (2013a)

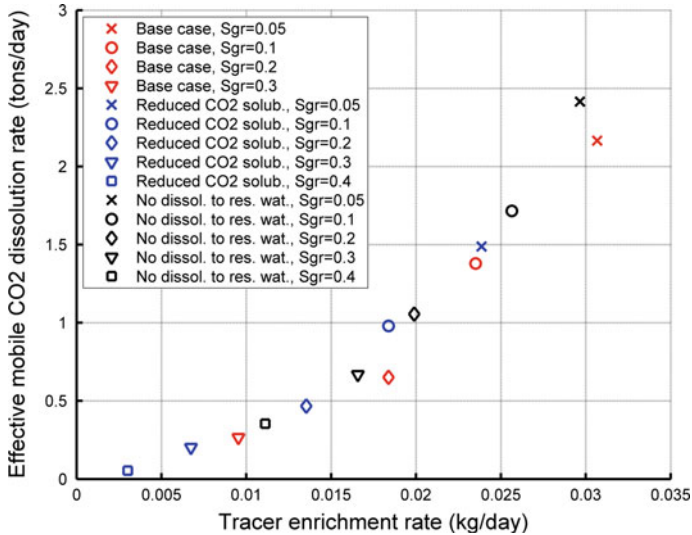


Fig. 7.23 Relationship between dissolution rate of mobile free-phase CO₂ and rate of tracer enrichment in the abstracted free-phase CO₂. From Fagerlund et al. (2013a)

simulated dissolution of the mobile free-phase CO₂ in the formation. This is illustrated in Fig. 7.23 which shows the dissolution of mobile CO₂ as a function of the tracer enrichment rate defined as the amount rate of tracer abstraction above the original injected concentration in the simulation study by Fagerlund et al. (2013a). Combining information about the total dissolution of CO₂ with dissolution of mobile CO₂, also the dissolution of residually trapped CO₂ can be estimated and the dissolution of trapped and mobile CO₂ can be separated.

In the aforementioned study, this tracer method was explored by numerical simulation for a small CO₂ injection (1000 tonnes of CO₂) and a relatively short test period. This test is too short to detect a convective dissolution process. However, with a long enough test period and favourable conditions (high permeability) to get onset of convective mixing, this type of tracer could potentially be used also to quantify the rate of dissolution during convective mixing.

The simulation studies of two-well CO₂ injection experiments show that these tests have the potential to quantify both residual trapping and dissolution of CO₂ at the field scale. Two-well tests will sample a larger reservoir volume and are likely to be more influenced by geological heterogeneity as compared to single-well push-pull tests such those of Paterson et al. (2013a, b).

The experiences from field tests such as Frio (Doughty et al. 2008; see also Sect. 8.6) and Otway (Paterson et al. 2013a, b; Zhang et al. 2011; Myers et al. 2012) have shown that well-instrumented small scale CO₂ injections have the potential to provide valuable information about the CO₂ migration and fate in a storage formation. Given the challenges to access and monitor the flow and transport processes in kilometre-deep reservoirs, the collection of multiple different data set and data types appear to be a vital strategy to understand the fate of the injected CO₂ and constrain estimates of CO₂ migration and trapping properties. A key to the interpretation of the different data sets and data types is a carefully constructed process-based model including the flow and transport processes of interest. With such model the different data can be jointly interpreted, different hypotheses can be tested and inverse modeling techniques can be used to estimate model parameters and related uncertainties.

7.5 Geomechanical Characterization

Francois H. Cornet and Victor Vilarrasa

Geomechanical characterization is an important part of any CO₂ geological storage project as understanding the stress field and the geomechanical strength of the formation rocks is necessary in order to anticipate possible damage to formation rocks and/or induced seismicity.

The drilling of boreholes is an essential part of the characterization program that must be conducted before undertaking any significant large scale operation within a

geological formation. Boreholes provide knowledge of the geometry of the various structural elements involved as well as samples for laboratory testing.

Analysis of geomechanical properties from core samples is discussed in Chap. 6. Samples are, however, often perturbed by the sampling process and they typically provide a sample of the intact rock only. Boreholes provide means of comparing results from laboratory tests to in situ field observations. In addition, boreholes provide the opportunity for conducting in situ measurements all along the borehole length of interest and this is very useful for ascertaining the representativity and variability of point observations associated with laboratory tests on samples. We concentrate here on the geomechanical characterization that may be conducted in boreholes, either as stand-alone measurements, or in combination with results from laboratory measurements and other logs.

The section starts with the identification of geomaterials and the characterization of fracture fields and faults. We then discuss the determination of elastic properties and strength characteristics of the various geomaterials. We follow up with a brief review of techniques used for the evaluation of regional stress field from in situ tests in boreholes, with special consideration for the specific needs of underground CO₂ sequestration. Next, we proceed to discuss how in situ stress measurements may help validate hypotheses on the rheological properties of geomaterials. We finally conclude with a discussion of observed scale effects in rock geomechanical properties and introduce a new, still to be tested, procedure that could be used to characterize the geomechanical characteristics of the CO₂ storage formation and the caprock. Please note that the theoretical development of the expressions for the geomechanical relationships is given in Sect. 3.6.

7.5.1 Geomaterials, Fracture Fields and Faults

7.5.1.1 Geomaterials

We define a geomaterial as the continuous material equivalent to the various materials that fill up volumes of rocks over which mechanical properties are considered as being uniform and may be characterized by those of a Representative Elementary Volume (REV) (e.g. Cornet 2015, Chap. 1). Geomaterials are porous and often multiphase, i.e. the pore space is filled by one or more liquids as well as by gas. The solid phase itself may be very heterogeneous at scales smaller than that of the REV. The characterization of geomaterials involves the determination of their mineral composition (including clay content) and various fluids content, their porosity, their density, their electrical conductivity, among other properties. This is the domain of petrophysics and various logging techniques have been developed for determining relevant parameters from in situ observations (see also Sect. 7.2.2). We will hereafter assume that porosity, density, clay content are known for the various geomaterials intersected by boreholes.

7.5.1.2 Fracture Fields and Faults

In addition to geomaterials, great attention must be given to fracture fields and faults. Fractures may be defined as sub-planar structures with one dimension being orders of magnitude smaller than those in the two other directions. It is recognized that some characteristics of fractures (such as roughness, spacing, radius, thickness/aperture) have fractal dimensions and therefore cannot be apprehended with the concept of Representative Elementary Volume (e.g., Brown and Scholtz 1985; Schmittbuhl et al. 1995; Bonnet et al. 2001).

If fractures are large enough to completely intersect a characterization borehole, they are generally identified explicitly both because fractures are weakness planes and exhibit hydraulic properties that strongly differ from those of the surrounding geomaterial. In contrast, smaller fractures are not taken into account explicitly, but only implicitly, through specific characteristics of the equivalent geomaterial. The orientation of fractures (strike and dip, or dip and dip direction) is determined through examination of borehole wall images. These borehole wall images may be obtained either from ultrasonic televiewer logs or from electrical imaging logs. Values for dip and dip-direction are plotted on a Schmitt stereographic projection so as to identify fracture sets. Fracture sets are characterized by their mean direction (two angles) and associated standard deviation, where the dispersion of data may be characterized by a normal (Gaussian) Probability Density Function (e.g., Goodman 1989, Chap. 1; Einstein and Baker 1983; Dershowitz et al. 1998).

It should be pointed out that faults are not big fractures, but are generally made up of a fault core (gouge) surrounded by two highly fractured zones (e.g., Sibson, 1977; Sulem et al. 2004; Micarelli et al. 2006). Faults are commonly longer than 100 m and may reach thousands of kilometers. Faults that are longer than a few kilometers generally involve many branches (e.g., Manighetti et al. 2001; Davis et al. 2005). Faults are usually assimilated either to a single geomaterial with specific material properties or to a multimaterial system that may be characterized by combining borehole and laboratory observations (Sulem 2007; Lockner et al. 2009). The large scale geometry of faults is often identified by seismic profiles (see Sect. 7.2 and discussion hereafter).

7.5.2 *Dynamic Elastic Properties of Geomaterials and Their Spatial Variations*

Traditionally, elastic characteristics of geomaterials are measured both in the laboratory by testing specimens prepared from cores and in the field by sonic logs (e.g., Paillet and White 1982), and sometimes by vertical or oblique seismic profiles (VSP).

Simple *sonic logs* involve the recording of P and S waves (i.e. the compression and shear waves, respectively) at two different sensors situated about 30–50 cm

from each other and at about 2–3 m away from the source. However, specific equipment may involve multiple sources and multiple sensors for sampling different distances between source and receivers. Further, whilst the simplest equipment involves only arrival times detection, more sophisticated equipment delivers the complete recording of signals for time durations long enough to cover the arrivals of Stoneley waves after the P and S waves. Stoneley waves correspond to tube waves; they are very sensitive to fractures and faults and their attenuation is used sometimes as a means for measuring the hydraulic characteristics of fractures (Hardin et al. 1987; Winkler et al. 1989). Sources used in simple sonic logs generate essentially P waves, and the observed S waves are generated by reflections and/or refractions through surfaces of discontinuity. More elaborated sonic tools have been developed and operate two sources in perpendicular directions so as to generate S waves (dipole sources).

Seismic profiles involve vibratory sources located on ground surface and three component sensors that are coupled to the borehole casing, or directly to the rock in open-hole sections, at regular depth intervals along the borehole. Sonic logs and seismic profiles involve the measurement of both P wave and S wave velocities and correspond to dynamic measurements that depend on the frequency of the excitation (from ten to twenty kiloHertz for sonic logs, and a few tens of Hertz for seismic profiles). Elastic parameters derived from these observations, which involve strains in the order of 10^{-6} or smaller, are generally referred to as dynamic properties. Sonic logs are much easier to run (and also much less costly) than seismic profiles as well as much more commonly used.

For isotropic materials, the shear modulus G and the Poisson's ratio ν are given by

$$G = \rho_B V_S^2 \quad (7.5.1)$$

$$\nu = \left[1 - 2(V_S/V_P)^2 \right] / 2 \left[1 - (V_S/V_P)^2 \right] \quad (7.5.2)$$

where V_P and V_S are the P and S wave velocities, respectively, and ρ_B is the geomaterial mean density.

Given the frequency of sonic logs (1–2 10^4 Hz), the wave lengths of the signals are in the range of a few tens of centimeters, so sonic logs may detect the presence of single fractures. For vertical or oblique seismic profiles, however, the frequency of the signal implies much longer wave lengths (in the range of a few hundred meters). Hence, for seismic profiles, a large number of fractures are included within one wave length and the measured velocity is generally much slower than that measured with sonic logs.

Elastic properties of fractures and microfissures may be characterized by a normal and a shear stiffness (e.g., Cornet 2015, Chap. 10). When these structures are randomly oriented in a material loaded under triaxial stress conditions, the equivalent material becomes stiffer in the maximum principal stress direction than in the minimum principal stress direction. This is also true for microcracks, and

extensive work has been done to discuss the effect of stress on microfractured rocks when they are modeled as equivalent anisotropic elastic solids (e.g., Nur 1971; Johnson and Rasolofosaon 1996; Zatsepin and Crampin 1997; Prioul et al. 2007). Randomly microfissured rock under triaxial stress loading conditions usually exhibits an orthorhombic (3 axes of symmetry) anisotropic behavior which implies 9 elastic constants. As a consequence, the velocity of shear waves depends on the relative orientation of their polarization direction with respect to that of the principal stress direction. Hence, the propagation of shear waves in an orthotropic material leads to the splitting into fast and slow shear waves. This phenomenon is known as shear wave splitting, or as the birefringence of shear waves.

Because VSP's involve much longer wave lengths than sonic logs do, they are dependent not only on the density of the microcracks, but also on that of the natural fractures. Experience has shown that the identification of fast and slow shear waves in VSP's may be used for identifying principal stress directions (e.g., Gaucher et al. 1998).

Borehole Seismic profiles are well suited for identifying major faults, not only through the associated local variation in wave velocity but mostly because faults are strong reflectors of both P and S waves (e.g., Place et al. 2011). VSP's have revealed also very useful for identifying limits between the various geomaterials through the reflected waves generated by the corresponding material interfaces and the various arrivals of refracted waves.

7.5.2.1 Strength Characterization

Laboratory measurements of elastic parameters involve the measurement of displacements generated by the application of external loads on specially prepared specimens loaded under uniaxial or triaxial compression conditions. The constant loading rates used for laboratory testing varies commonly between 10^{-4} and 10^{-6} % per second so that laboratory measurements are often referred to as quasi-static measurements. They always yield much lower elastic moduli than do dynamic measurements, unless the minimum principal stress is very high (larger than 100 MPa). This demonstrates that rocks are not linearly elastic and the dependence on time implies some viscosity for the geomaterial behavior. The fact that the discrepancy between quasi-static and dynamic properties decreases as the minimum principal stress applied on the rock becomes larger suggests that the main source of the discrepancy is linked to the mechanical behavior of the discontinuities (micro-fissures and fractures). Micro-fissures and fractures also control the "strength" of these materials, i.e., the stress conditions at which failure develops. Hence, many investigations have been conducted for evaluating whether the difference between dynamic and quasi-static measurements may be combined with the value of the dynamic Young's modulus together with other parameters like the clay content for evaluating the "strength" of the rock. Here the concept of strength refers to the Coulomb failure criterion.

This practice has been developed in the oil industry for the design of drilling operations in sedimentary rocks in order to avoid borehole collapse. An extensive review of these various empirical relationships has been proposed by Chang et al. (2006) for estimating the Unconfined Compressive Strength (UCS) and the intrinsic friction angle implied by the Coulomb failure criterion for sandstones, shales, limestones and dolomite.

However, it should be kept in mind that these empirical relationships are meant to prevent the collapse of boreholes during drilling. They do not provide “strength” data for the safe design of long term CO₂ sequestration schemes. We recommend performing laboratory and field tests to determine the strength site specifically.

7.5.3 Regional Stress Field Evaluation

A crucial part of the design of a CO₂ sequestration project is the identification of the maximum fluid pressure that may be reached during the various injection phases. This is required first so as not to create any hydraulic fracture within the reservoir and second, to avoid leaks through the caprock. Another important issue is the control of induced seismicity. This implies understanding fluid diffusion not only within the aquifer but also in the overlying and underlying geological formations.

These various design considerations require a sound understanding of the regional stress field in the caprock, the aquifer, and the underlying geological formation. An efficient microseismic monitoring, during and after all main injection phases, is required to detect any possible induced seismicity, with particular attention to the growth direction of the microseismic cloud. Here, we only discuss the determination of the regional stress field, i.e., the identification of principal stress directions together with the magnitude of principal stress components for the caprock, the aquifer and the underlying geological formations. These may be evaluated through various techniques that we discuss below.

7.5.3.1 Stress Evaluation from Sonic Logs

The drilling of a borehole in a stressed geological material results in local stress concentrations around the borehole up to distances equal to about 4–5 times the borehole radius (e.g., Cornet 2015). If one of the principal stress components is parallel to the borehole axis (often this is the vertical direction, so that the corresponding principal stress magnitude is called σ_V), then the two other principal stress directions are normal to the borehole axis and are referred to as σ_H and σ_h , with the convention $\sigma_H > \sigma_h$. For such geometry, the tangential stress component, $\sigma_{\theta\theta}$ at the borehole wall is

$$\sigma_{\theta\theta} = (\sigma_H + \sigma_h) - 2(\sigma_H - \sigma_h) \cos \theta, \quad (7.5.3)$$

where θ is the angular coordinate defined with respect to the σ_H direction. $\sigma_{\theta\theta}$ varies from $(-\sigma_H + 3\sigma_h)$ in the maximum horizontal principal stress direction to $(-\sigma_h + 3\sigma_H)$ in the minimum principal stress direction. As pointed out above, the elastic constants of a geomaterial depend on the stress field, and the directions of axes of symmetry of the elastic anisotropy correspond to those of the principal stress components, if the rock is isotropic when it is completely unloaded.

This property used in sonic logs conducted with dipole sources for identifying both the directions and the magnitudes of the far-field principal stress components (Lei et al. 2012). Preliminary results from field tests showed good agreement with results from hydraulic tests. However, it should be pointed out that, currently, such measurements are not routinely conducted.

7.5.3.2 Stress Evaluation from Borehole Wall Images (Borehole Breakouts Orientations)

As shown by Eq. (7.5.3), the tangential stress component at the borehole wall varies with the angular coordinate of the point under consideration and takes a particularly simple form in terms of horizontal principal stress magnitudes for vertical boreholes, when the vertical direction is also a principal stress direction. It reaches its maximum value for $\theta = \pi/2$ and $\theta = 3\pi/2$, i.e., in the direction of the minimum horizontal principal stress.

The magnitudes of the far-field principal stress components, i.e., away from the wellbore, increase with depth, and when the tangential stress, at the wellbore wall, reaches the compressive strength of the material, failure occurs.

Hence, when borehole wall images are available (preferentially ultrasonic borehole images, but also electrical borehole images), zones of borehole failure (called borehole breakouts) caused by too large far-field stress magnitudes can be observed at two symmetrical locations. These locations are aligned with the minimum principal stress direction (e.g., Zoback et al. 2003).

Because the compressive strength of shales is much lower than that of limestones and sandstones, borehole breakouts are first detected in these soft formations. Some attempts have been made to extract from the width of borehole breakout the principal stress magnitudes. It should be pointed out, however, that for some materials, like shale or clay, the compressive strength depends on many factors including the composition of the drilling mud. Furthermore, the drill string assembly usually includes, at some distance above the cutting tool, so called reamers that keep the borehole at the required shape so that borehole diameters may not depend solely on far field stress magnitudes. Hence it is considered that borehole breakouts are very reliable markers of the principal stress directions, but not of the principal stress magnitudes.

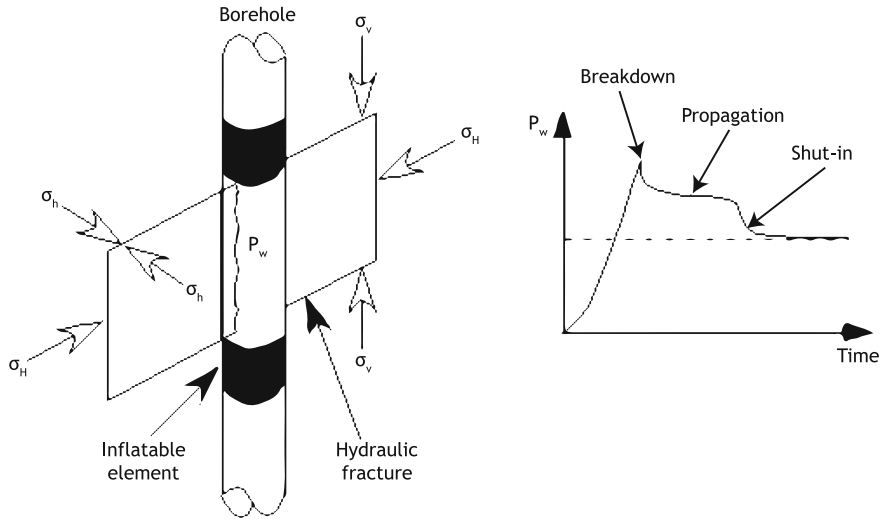


Fig. 7.24 Stress measurement by hydraulic fracturing. *Left* principle of the method; *right* typical pressure-time record

7.5.3.3 Stress Evaluation from Hydraulic Tests in Boreholes (HF and HTPF)

The most robust method for determining in situ stresses from boreholes is by hydraulic tests, with inflatable straddle packers that isolate portions of a borehole (see Fig. 7.24) (Haimson and Cornet 2003). Like borehole breakouts, the method is based on Eq. (7.5.3) that shows that the minimum tangential stress at the borehole wall is in the direction of the far field maximum stress direction, when the borehole is parallel to a principal stress direction. When water pressure P_w is applied to the borehole wall, it generates at all points of the borehole wall a negative tangential stress component equal in magnitude to the applied pressure (compressions are reckoned positive). When the tangential stress reaches the tensile strength of the rock, σ^T , a tensile rupture occurs in the direction of the maximum horizontal principal stress (Fig. 7.24)

$$\sigma_{\theta\theta} = -\sigma_H + 3\sigma_h - P_w = \sigma^T. \tag{7.5.4}$$

On the right panel of the figure it can be seen that, when a fluid is injected at a constant flow rate in between the two inflatable packers, the pressure first rises linearly. Then a peak is reached (breakdown pressure) that is classically considered to correspond to the initiation of hydraulic fracturing. However recent work has shown that the fracture initiates below the packers, for an interval pressure lower than the breakdown pressure. Hence the pressure to be considered for the initiation of fracture is that of the packer when the record of interval pressure versus time gets non-linear.

The fracture initiation pressure and the shut-in pressure may be used to determine both the maximum and the minimum principal stress magnitudes. For HTPF tests (hydraulic testing on pre-existing fractures), the straddle packer is set up on a portion of the borehole where a single pre-existing fracture exists. Then, a slow injection of fluid into the fracture leads to its mechanical opening and the shut-in pressure observed at the end of testing yields a direct measurement of the normal stress applied to the fracture away from the well bore.

Combinations of HF (hydraulic fracturing) and of HTPF yield redundant measurements that help constraining efficiently all the components of the stress field away from the borehole.

7.5.4 Vertical Stress Profiles and the Characterization of the Rheology of Geomaterials

The magnitude of all principal stress components generally increases linearly with depth when stress measurements are conducted in homogeneous formations like granite. But when measurements are conducted in sedimentary formations, which are relevant for geological storage of CO₂, the measured stress magnitudes are found to depend very strongly on the nature of the materials. In particular, it is well recognized that the magnitude of the differential stress ($\sigma_H - \sigma_h$) is much smaller in soft materials, such as shale and evaporites, than in relatively stiff materials like sandstone or limestone (e.g., Cornet and Röckel 2012).

Some attempts have been made at determining the elastic parameters of these formations through numerical modeling (Gunzburger and Magnenet 2014). Such modeling assumes an elastic behavior for the material over millions of years. However, the very fact that dynamic, quasi-static and static elastic measurements may differ markedly, as discussed in Sect. 7.5.2, clearly demonstrates that the hypothesis of a constant value for the elastic parameters independent of time is not valid (Gunzburger 2010).

Various attempts are presently undertaken at evaluating this time dependency (e.g., Sone and Zoback 2014; Cornet 2015), and it is hoped that such approaches will develop further so as to produce reliable values for time scales ranging from thousands to tens of thousands years.

7.5.5 Scale Effects of the Mechanical Properties

As discussed above, mechanical properties of rocks are usually inferred from core samples at the laboratory. These values may not be representative at the field scale because of the existence of fissures, vugs, joints or fractures, which are more deformable than the intact rock that usually constitute core samples. This is

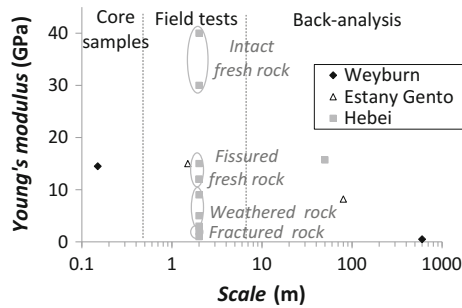


Fig. 7.25 Values of Young's modulus as a function of scale. Three case studies of mechanical properties determination at different scales are included. The rock results softer in back-analysis than in core samples measurements and field tests because of the presence of an increasing number of deformable fractures as the scale increases. The case studies refer to Estany Gento, Spain (gneiss) (Ledesma et al. 1996), Hebei, China (andesite) (Zhang et al. 2006) and Weyburn, Canada (limestone) (Verdon et al. 2011)

illustrated by the dependence of the Young's modulus on the scale of measurement (Fig. 7.25). Figure 7.25 displays three case studies [a cavern excavation in Estany Gento, Spain (Ledesma et al. 1996), a gallery excavation in Hebei, China (Zhang et al. 2006) and CO₂ injection at Weyburn, Canada (Verdon et al. 2011)] in which the Young's modulus is measured at the laboratory from core samples (intact rock), on a rock surface in the field with a flat jack test (meter scale on a variety of rock conditions) and inferred from back-analysis of convergence measurements in underground excavations or microseismicity measurements induced by CO₂ injection (field scale). The results show that field scale values of Young's modulus are much smaller than those obtained from core samples or field tests, typically performed in competent rock. The lower Young's modulus values suggest that rocks become softer for increasing scale. This reflects the fact that discontinuities, which are much more deformable than intact rock, play a major role in the mechanical behavior of the rock mass. Nevertheless, for the case of Hebei, hydraulic jack tests were performed on rock surfaces of varying quality, yielding a wide range of Young's modulus. Therefore, the resulting Young's modulus from the back-analysis of the convergence measurements of a gallery excavation gave an average value representative of the whole rock mass.

The Weyburn case study is a relevant example of scale effects on the mechanical properties in CO₂ storage. Verdon et al. (2011) presented the induced seismicity recorded in the Weyburn CO₂ Storage and Monitoring Project and built up a representative geomechanical model of the CO₂ injection. The model simulates the changes in the effective stress field induced by CO₂ injection and predicts the generation of microseismic events. As microseismic activity is directly linked with induced effective stress changes, it can be used to constrain geomechanical models. The first numerical model they performed used material properties based on laboratory core measurements and did not yield a good match with microseismic

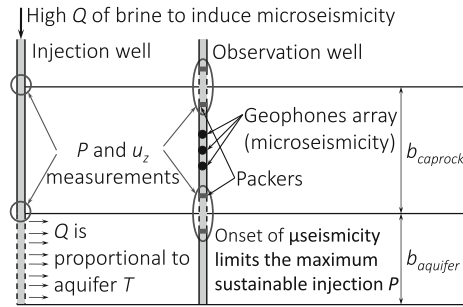


Fig. 7.26 Schematic representation of the hydromechanical characterization test by Vilarrasa et al. (2013). A sufficiently high water flow rate capable of reaching the maximum sustainable injection pressure is injected for several hours. Fluid pressure and displacements or strains should be monitored in the aquifer and caprock in as many places as possible (preferably in both the injection and the observation well(s), but at least in one well)

observations. They found that an alternative model reducing the stiffness by one order of magnitude with respect to the laboratory measurements gives a good correlation with the observed microseismic events.

These examples illustrate that the large-scale geomechanical properties are difficult to quantify (Rutqvist 2012). To address this difficulty, Vilarrasa et al. (2013) have proposed a field test to characterize the macroscopic mechanical properties of the rock layers involved in CO₂ storage in deep geological formations. It should be pointed out that this test has not yet been implemented in the field and is therefore taken here as a conceptual example to characterize the hydromechanical properties rather than an example of how to do a field test. The proposed hydromechanical characterization test consists in injecting water at high pressure, while monitoring fluid pressure, rock deformation and induced microseismicity (Fig. 7.26). The overpressure (several MPa) is proportional to the flow rate, which may become high if the aquifer transmissivity is high. The injected water can be obtained from surface sources, e.g., rivers or lakes. However, aquifer brine must be used if geochemical alteration is not desired. In this case, brine should be pumped and stored at the surface prior to the injection test and leave enough time to recover pre-pumping pressure levels in the aquifer.

The instrumentation for the hydromechanical characterization test consists of equipment to measure fluid pressure, vertical displacement and microseismicity. Fluid pressure and vertical displacement measurements are taken in the injection and observation wells, both in the aquifer and the caprock (Fig. 7.26). Fluid pressure should be measured using pressure transducers located between two packers to isolate an interval of the well that must be in hydraulic contact with the rock. Temperature measurements, which can be made with a fiber-optic (see Sect. 8.4), can be also useful to account for thermal effects if the injected water is not in thermal equilibrium with the storage formation. Vertical displacements in deep boreholes are not easy to measure. Alternatively, strain measurements with

fiber-optic can be used. However, it is still difficult to say what deformation is being measured because the measuring equipment will be embedded in the cement between the casing and the rock, which are of different stiffness, and thus deform differently. To detect and locate microseismic events of magnitudes as low as -2 , an array of geophones should be placed in the observation well at depth. The distribution of the geophones should be carefully designed to permit distinguishing induced microseismicity from background noise and locating hypocenters with high accuracy (<100 m) (IEAGHG 2013). Additionally, a network of seismographs in surface can complement the microseismicity measurements and help to localize the events..

During the test, overpressure should be progressively increased until the elastic limit is reached and microseismicity is triggered. The initial induced microseismicity still occurs in the elastic domain and can be related to the Kaiser effect (Cornet 2012, 2016). Induced microseismic events may take place both in the aquifer and the caprock. Since microseisms are associated with shear slip, which opens up fractures and enhances their transmissivity, microseismicity will be beneficial if it occurs within the aquifer. Microseismicity should, however, be avoided in the caprock as it may jeopardize caprock integrity. Thus, overpressure should be immediately decreased if microseismic events are induced in the caprock to avoid compromising the caprock sealing capacity. The onset of microseismicity in the caprock can be used as an indicator of the overpressure that must not be exceeded during the operational stage of CO_2 injection.

The characterization of the hydromechanical properties of the aquifer and the caprock is done from pressure and displacement or strain measurements in both rock formations. The hydraulic properties, i.e., aquifer transmissivity and storage coefficient, can be estimated from the interpretation of fluid pressure evolution (Cooper and Jacob 1946). The mechanical properties, i.e., Young’s modulus and Poisson ratio, of the aquifer and the caprock can be estimated by introducing field

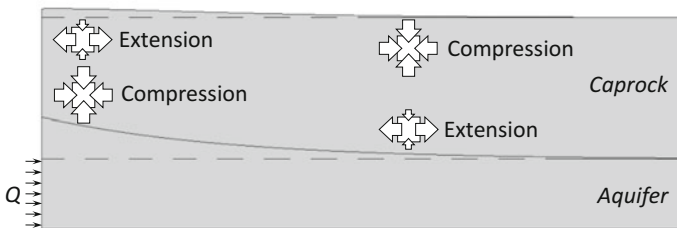


Fig. 7.27 Original (*dashed lines*) and deformed (*continuous lines*) form of the aquifer and the whole caprock when injecting a fluid in the aquifer. The uplift at the *top* of the aquifer generates compression in the *lower part* of the caprock close to the injection well and extension far away from it. However, extension appears in the *upper part* of the caprock close to the well and compression far away from it. While the pore volume decreases where the caprock is compressed, it increases where the caprock extends. Fluid pressure in the caprock is inversely proportional to the volumetric strain change. Thus, fluid pressure increases where the pore volume decreases and decreases where the pore volume increases

measurements in dimensionless plots developed by Vilarrasa et al. (2013). These plots include curves for overpressure and vertical displacement as a function of the volumetric strain term obtained from a dimensional analysis of the hydromechanical equations.

The reason for measuring fluid pressure in the caprock lies in the coupled hydromechanical effect that occurs during injection. When injecting a fluid in an aquifer, fluid pressure increases, changing the effective stress field. This produces an expansion of the aquifer. Vertical displacement presents a shape similar to that of fluid overpressure at the top of the aquifer, which decreases logarithmically with distance. As a result, the caprock is also deformed (Fig. 7.27). The vertical displacement does, however, become smoother at the top of the caprock, because the caprock acts as a spring, dissipating the deformation of the aquifer. But the pressure buildup propagation from the aquifer into the caprock is orders of magnitude slower than that of the aquifer due to the permeability contrast between the two formations. This means that the overpressure caused by injection only affects the first meters of the lower part of the whole caprock. However, fluid pressure changes occur in the whole caprock due to volumetric strain variations caused by caprock deformation (Fig. 7.27).

The uplift at the top of the aquifer generates compression in the lower part of the caprock close to the injection well, so fluid pressure increases. Extension appears at the top of the caprock close to the well, which increases the pore volume and thus fluid pressure decreases. This leads to a reverse-water level fluctuation, which is well-documented in confined aquifers. When fluid is pumped, hydraulic heads in adjacent aquitards rise after pumping starts (Rodrigues 1983; Hsieh 1996; Kim and Parizek 1997). This phenomenon is known as “reverse-water level fluctuation” or “Noordbergum effect”, because it was observed for the first time in the village of Noordbergum, the Netherlands (Verruijt 1969). Since in CO₂ sequestration a fluid is injected, an opposite response to that observed in Noordbergum occurs, i.e., fluid pressure drops in the upper part of caprock in the vicinity of the injection well (Vilarrasa et al. 2010). The contrary occurs far away from the injection well, i.e., extension at the lower part of the caprock and compression at its top. These effects are, however, small compared to those close to the well.

References

- Agnet N, Moradi-Tehrani N, Tillement O (2011) Fluorescent nanobeads: a new generation of easily detectable water tracers. *Procs Int Petrol Technol Conf, IPTC 15312*
- Aki K, Richards P (1980) *Quantitative seismology*. University Science Books
- Alcalde J, Martí D, Calahorrano A, Marzan I, Ayarza P, Carbonell R, Juhlin C, Pérez-Estaún A (2013) Active seismic characterization experiments of the Hontomín research facility for geological storage of CO₂, Spain. *Int J Greenhouse Gas Control* 19:785–795
- Alcolea A, Carrera J, Medina A (2006) Pilot points method incorporating prior information for solving the groundwater flow inverse problem. *Adv Water Resour* 29(11):1678–1689
- Anderson MP (2005) Heat as a ground water tracer. *Ground Water* 43(6):951–968

- Annable MD, Rao PSC, Hatfield K, Graham WD, Wood AL, Enfield CG (1998) Partitioning tracers for measuring residual NAPL: field-scale test results. *J Environ Eng* 124:498–503
- Bear J (1988) *Dynamics of fluids in porous media*. Dover, New York
- Becker MW, Reimus PW, Vilks P (1999) Transport and attenuation of carboxylate-modified latex microspheres in fractured rock laboratory and field tracer tests. *Ground Water* 37:387–395
- Becker MW, Metge DW, Collins SA, Shapiro AM, Harvey RW (2003) Bacterial transport experiments in fractured crystalline bedrock. *Ground Water* 41:682–689
- Bennett B, Larter SR (1997) Partition behaviour of alkylphenols in crude oil/brine systems under subsurface conditions. *Geochim Cosmochim Acta* 61:4393–4402
- Behrens H, Ghergut I, Sauter M (2010) Tracer properties, and tracer test results—part 3: modification to shock's flow-storage diagram method. Presented at the thirty-fifth workshop on geothermal reservoir engineering, Stanford University, SGP-TR-188
- Behrens H, Ghergut J, Bensabat J, Niemi A, Sauter M (2014) Merging single- and inter-well tracer tests into one forced-gradient dipole test, at the Heletz site within the MUSTANG project. *Energy Procedia* 59:249–255
- Bonnet E, Bour O, Odling NE, Davy P, Main I, Cowie P et al (2001) Scaling of fracture systems in geological media. *Rev Geophys* 39:347–383
- Bourdet D, Whittle TM, Douglas AA, Pirard YM (1983) A new set of type curves simplifies well test analysis. *World Oil* 196:95–106
- Bourdet D, Ayoub JA, Pirard YM (1989) Use of pressure derivative in well-test interpretation. *SPE Repr Ser* 4:293–302
- Brown SR, Scholtz CH (1985) Broad bandwidth study of the topography of natural rock surfaces. *J Geophys Res* 90:12575–12582
- Carrera J, Sánchez-Vila X, Benet I, Medina A, Galarza G, Guimerà J (1998) On matrix diffusion: formulations, solution methods and qualitative effects. *Hydrogeol J* 6:178–190
- Chang C, Zoback MD, Khaksar A (2006) Empirical relations between rock strength and physical properties in sedimentary rocks. *J Petrol Sci Eng* 51:223–237
- Chow VT (1952) On the determination of transmissibility and storage coefficients from pumping test data. *Trans Am Geophys Union* 33:397–404
- Cooper HH, Jacob CE (1946) A generalized graphical method for evaluating formation constants and summarizing well field history. *Am Geophys Union Trans* 27:526–534
- Cornet FH (2015) *Elements of crustal geomechanics*. Cambridge University Press, Cambridge
- Cornet FH (2016) Seismic and aseismic motions generated by fluid injections. *Geomech Energy Environ* 5:42–54
- Cornet FH, Röckel T (2012) Vertical stress profiles and the significance of stress decoupling. *Tectonophysics* 581:193–205
- Davis BM, Istok JD, Semprini L (2002) Push–pull partitioning tracer tests using radon-222 to quantify non-aqueous phase liquid contamination. *J Contam Hydrol* 58:129–146
- Davis K, Burbank DW, Fisher D, Wallace S, Nobes D (2005) Thrust fault growth and segment linkage in the active Ostler fault zone, New Zealand. *J. Struct Geol* 27:1528–1546
- Dean C, Reimus P, Newell, D (2012) Evaluation of a cation exchanging tracer to interrogate fracture surface area in EGS systems. In: *Proceedings, 37th Workshop on Geothermal Reservoir Engineering*, Stanford, CA
- Deeds, NE, McKinney, Pope, GA, (1999) Vadose zone characterization at a contaminated field site using partitioning interwell tracer technology. *Environ Sci Technol* 33:2745–2751
- Dershowitz W, La Pointe P, Cladouhos T (1998) Derivation of fracture spatial pattern parameters from borehole data. *Int J Rock Mech Min Sci* 35(4/5):508
- Divine CE, McDonnell JJ (2005) The future of applied tracers in hydrogeology. *Hydrogeol J* 13:255–258
- DNV (2010) DNV CO2QUAL: guideline for selection and qualification of sites and projects for geological storage of CO₂. http://www.dnv.com.au/binaries/CO2QUALSTORE_guideline_tcm162-412142.pdf
- Doughty C, Freifeld BM, Trautz RC (2008) Site characterization for CO₂ geologic storage and vice versa—the Frio brine pilot, Texas, USA as a case study. *Environ Geol* 54(8):1635–1656

- Du Y, Guan L (2005) Inter-well tracer tests: lesson learned from past field studies. Soc Pet Eng SPE paper 93140
- Edlmann K, Edwards MA, Qiao XJ, Haszeldine RS, McDermott CI (2014) Appraisal of global CO₂ storage opportunities using the geomechanical facies approach. Environmental earth sciences. Springer, New York
- Einstein HH, Baecher GB (1983) Probabilistic and statistical methods in engineering geology; Rock mech. Rock Eng 84:366–376
- Ennis-King J, Paterson L (2005) Role of convective mixing in the long-term storage of carbon dioxide in deep saline formations. Soc Pet Eng SPE paper 84344
- Erlström M, Silva O, Vries LM, Shtivelman V, Gendler M, Goldberg I, Scadeanu D, Sperber CM (2010) 3D structures of the test sites. Deliverable D2.2. MUSTANG (a multiple space and time scale approach for the quantification of deep saline formations for CO₂ storage) EU FP7 project report. Nov 2010. www.co2mustang.eu
- Erlström M, Rötting T, Sperber CM, Shtivelman V, Scadeanu D, Sperber CM (2011) Report on property values and parameters, related uncertainties. Deliverable D2.3. MUSTANG (a multiple space and time scale approach for the quantification of deep saline formations for CO₂ storage) EU FP7 project report. Deliverable D2.2 July 2011. www.co2mustang.eu
- EU (2009) Directive 2009/31/EC of the European parliament and the council of 23 April 2009, on the geological storage of carbon dioxide and amending council directive 85/337/EEC, European parliament council directives 2000/60/EC, 2001/80/EC, 2004/35/EC, 2006/12/EC, 2008/1/EC and regulation no. 101/2006, App 1. Criterial for the site characterization and assessment of the potential storage complex and the surroundings
- Fagerlund F (2007) Experimental and modeling studies on the spreading of non-aqueous phase liquids in heterogeneous media. PhD Thesis, Uppsala University
- Fagerlund F, Niemi A, Bensabat J, Shtivelman V (2013a) Design of a two-well field test to determine in-situ residual and dissolution trapping of CO₂ applied to the Heletz CO₂ injection site. Int J Greenhouse Gas Control 19:642–651
- Fagerlund F, Niemi A, Bensabat J, Shtivelman V (2013b) Inter-well field test to determine in-situ CO₂ trapping in a deep saline aquifer: modelling study of the effects of test design and geological parameters. Energy Procedia 40:554–563
- Flett M, Gurton R, Weir G (2007) Heterogeneous saline formations for carbon dioxide disposal: impact of varying heterogeneity on containment and trapping. J Pet Sci Eng 57:106–118
- Freifeld BM, Finsterle S, Onstott TC, Toole PLMP (2008) Groundsurface temperature reconstructions: using in situ estimates for thermal conductivity acquired with a fiber-optic distributed thermal perturbation sensor. Geophys Res Lett 35:L14309
- Gaucher E, Cornet FH, Bremard P (1998) Induced seismicity analysis for structure identification and stress field determination; SPE paper SPE-47324, pp 545–554 of Euroc-98, Soc Pet Eng
- Ghergut I, Behrens H, Maier F, Karmakar S, Sauter M (2011) A note about “heat exchange areas” as a target parameter for SWIW tracer tests. In: Stanford geothermal program workshop report SGP-TR-191, pp 303–312
- Ghergut J, Behrens H, Sauter M, Licha T, Nottebohm M (2013) Can Peclet numbers depend on tracer species? Going beyond SW test insensitivity to advective or equilibrium-exchange processes. In: Stanford geothermal workshop proceedings, SGP-TR-198, pp 326–335
- Giese R, Hennings J, Lüth S, Morozova D, Schmidt-Hattenberger C, Würdemann H, Zimmer M, Cosma C-G, Juhlin C, CO₂SINK Group (2009) Monitoring at the CO₂SINK site: a concept integrating geophysics, geochemistry and microbiology. Energy Procedia 1(1):2251–2259
- Goodman RE (1989) Introduction to rock mechanics. Wiley, New York
- Green C, Ennis-King J, Pruess K (2009) Effect of vertical heterogeneity on long-term migration of CO₂ in saline formations. Energy Procedia 1:1823–1830
- Gunzburger Y (2010) Stress state interpretation in light of pressure-solution creep: numerical modelling of limestone in the Eastern Paris Basin, France. Tectonophysics 483(3):377–389
- Gunzburger Y, Magenet V (2014) Stress inversion and basement-cover stress transmission across weak layers of the Paris Basin, France. Tectonophysics 617:44–57

- Haggerty R, Fleming SW, Meigs LC, McKenna SA (2001) Tracer tests in a fractured dolomite: 2. Analysis of mass transfer in single-well injection-withdrawal tests. *Water Resour Res* 37:1129
- Haimson BC, Cornet FH (2003) ISRM suggested methods for rock stress estimation—part 3: hydraulic fracturing (HF) and/or hydraulic testing of preexisting fractures (HTPF). *Int J Rock Mech Min Sci* 40:1011–1020
- Hallam A (1981) *Facies Interpretation and the stratigraphic record*: freeman, p 291
- Hantush MS, Jacob CE (1955) Non-steady radial flow in an infinite leaky aquifer. *Trans Am Geophys Union* 36:95–100
- Hardin EL, Cheng C, Paillet FL, Mendelson JD (1987) Fracture characterization by means of attenuation and generation of tube waves in fractured crystalline rock at Mirror lake, New Hampshire. *J Geophys Res* 92:7989–8006
- Hasan AR, Kabir CS (2002) *Fluid flow and heat transfer in wellbores*. Society of Petroleum Engineers, Richardson, TX
- Hillebrand O, Nödler K, Licha T, Sauter M, Geyer T (2012) Identification of the attenuation potential of a karst aquifer by an artificial dualtracer experiment with caffeine. *Water Res* 46:5381–5388
- Hesse MA, Orr FM Jr, Tchelepi HA (2009) Gravity currents with residual trapping. *Energy Procedia* 1:3275–3281
- Hovorka S, Doughty C, Benson SM, Pruess K, Knox PR (2004) The impact of geological heterogeneity on CO₂ storage in brine formations: a case study from the Texas Gulf Coast. In: Bains SJ, Worden RH (eds) *Geological storage of carbon dioxide*, vol 233. Geological Society of London, Special Publications, pp 147–163
- Hovorka SD, Benson SM, Doughty C, Freifeld BM, Sakurai S, Daley TM, Kharaka YK, Holtz MH, Trautz RC, Nance HS, Meyer LR, Knauss KG (2006) Measuring permanence of CO₂ storage in saline formations—the Frio experiment. *Environ Geosci* 13(2):105–121
- Hsieh PA (1996) Deformation-induced changes in hydraulic head during ground-water withdrawal. *Ground Water* 34(6):1082–1089
- Hunkeler D, Hoehn E, Höhener P, Zeyer J (1997) 222Rn as a partitioning tracer to detect diesel fuel contamination in aquifers: laboratory study and field observations. *Environ sci technol* 31(11):3180–3187
- IEAGHG (2013) *Induced seismicity and its implications for CO₂ storage risk*, 2013/09
- Istok JD, Humphrey MD, Schroth MR, Hyman MR, O'Reilly KT (1997) Single-well, push–pull test for in situ determination of microbial activities. *Ground Water* 35:619–631
- Istok JD, Field JA, Schroth MH, Dwarakanath V (2002) Single-well “push–pull” partitioning tracer test for NAPL detection in the subsurface. *Environ Sci Technol* 36:2708–2716
- Jin M, Delshad M, Dwarakanath V, McKinney DC, Pope GA, Sepehrnoori K, Tilburg CE, Jackson RE (1995) Partitioning tracer test for detection, estimation, and remediation performance assessment of subsurface nonaqueous phase liquids. *Water Resour Res* 31:1201–1211
- Johnson PA, Rasolofosaon PNJ (1996) Non-linear elasticity and stress induced anisotropy I rock. *J Geophys Res* 101:3113–3124
- Juhlin Ch, Giese R, Zinck-Jørgensen K, Cosma C, Kazemeini H, Juhonjuntti N, Lüth S, Norden B, Förster A (2007) 3D baseline seismics at Ketzin, Germany: the CO₂SINK project. *Geophysics* 72(5):B121–B132
- Juliusson E, Horne RN (2010) Study and simulation of tracer and thermal transport in fractured reservoirs. In: *Proceedings, 35th workshop on geothermal reservoir engineering*, Stanford University, Stanford, CA, SGP-TR-188
- Jung Y, Pruess K (2012) A closed-form analytical solution for thermal single-well injection-withdrawal tests. *Water Resources Research* 48 doi:[10.1029/2011WR010979](https://doi.org/10.1029/2011WR010979)
- Kazemeini S, Juhlin C, Fomel S (2010) Monitoring CO₂ response on surface seismic data; a rock physics and seismic modeling feasibility study at the CO₂ sequestration site, Ketzin, Germany. *J Appl Geophys* 71:109–124
- Keswick BH, Wang D-S, Gerba CP (1982) The use of microorganisms as ground-water tracers: a review. *Ground Water* 20:142–149

- Kim J-M, Parizek RR (1997) Numerical simulation of the Noordbergum effect resulting from groundwater pumping in a layered aquifer system. *J Hydrol* 202:231–243
- Kim H, Annable MD, Rao PSC (1998) Influence of air-water interfacial adsorption and gas-phase partitioning on the transport of organic chemicals in unsaturated porous media. *Environ Sci Technol* 32:1253–1259
- Kneafsey T, Pruess K (2010) Laboratory flow experiments for visualizing carbon dioxide-induced, density-driven brine convection. *Transp Porous Media* 82(1):123–139
- Knudby C, Carrera J (2005) On the relationship between indicators of geostatistical, flow and transport connectivity. *Adv Water Resour* 28(4):405–421
- Kocabas I (2005) Geothermal reservoir characterization via thermal injection-backflow and inter-well tracer testing. *Geothermics* 34:27–46
- Kocabas I, Maier F (2013) Analytical and numerical modeling of tracer flow in oil reservoirs containing high permeability streaks. In: *SPE middle east oil and gas show and conference*, 10–13 Mar 2013, Manama, Bahrain
- Kruseman GP, de Ridder NA (1994) *Analysis and evaluation of pumping test data*, 2nd edn. ILRI publication 47, Wageningen, The Netherlands, p 377
- LaForce T, Ennis-King J, Boreham C, Paterson L (2014) Residual CO₂ saturation estimate using noble gas tracers in a single-well field test: the CO₂CRC Otway project. *Int J Greenhouse Gas Control* 26:9–21
- Land CS (1968) Calculation of imbibition relative permeability for two- and three phase flow from rock properties. *Soc Petrol Eng J Trans Am Inst Min Metall Pet Eng* 243:149–156
- Lay T, Wallace T (1995) *Modern global seismology*, vol. 58. Academic Press, New York
- Ledesma A, Gens A, Alonso EE (1996) Parameter and variance estimation in geotechnical backanalysis using prior information. *Int J Numer Anal Meth Geomech* 20:119–141
- Leecaster K, Ayling B, Moffitt G, Rose P (2012) Use of safranin T a reactive tracer for geothermal reservoir characterization. In: *Proceedings, 37th Workshop on Geothermal Reservoir Engineering*, Stanford University, SGP-TR-194
- Lei T, Sinha BK, Sanders M (2012) Estimation of horizontal stress magnitudes and stress coefficients of velocities using borehole sonic data. *Geophys* 77(3), WA181–WA196
- Leibundgut C, Maloszewski P, Külls C (2009) *Tracers in hydrology*, Auflage: 1. Auflage. Wiley, Chichester, UK ; Hoboken, NJ
- Lockner DA, Tanaka H, Ito H, Ikeda R, Omura K, Naka H (2009) Geometry of the Nojima Fault at nojima-Hirabayashi, Japan-I. A simple damage structure inferred from borehole core permeability. *Pure App Geophys* 166:1649–1667
- Luo S, Xu R, Jiang P (2012) Effect of reactive surface area of minerals on mineralization trapping of CO₂ in saline aquifers. *Pet Sci* 9:400–407
- Maier F, Kocabas I (2013) Comment on “A closed-form analytical solution for thermal single-well injection-withdrawal tests” by Jung and Pruess. *Water Resour Res* 49(1):640–643
- Maier F, Oberdorfer P, Kocabas I, Ghergut I, Sauter M (2012) Using temperature signals to estimate geometry parameters in fractured geothermal reservoirs. In: *Proceedings, COMSOL Conference 2012, Milano, Italy*
- Maier F, Schaffer M, Nur SN, Licha T (2014) Ability of thermo-sensitive tracers for precisely estimating system temperatures in column experiments with thermal gradient. In: *Proceedings, 39th workshop on geothermal reservoir engineering*, Stanford University, Stanford, CA, SGP-TR-202
- Maloszewski P, Zuber A (1985) On the theory of tracer experiments in fissured rocks with a porous matrix. *J Hydrol* 79:333–358
- Maloszewski P, Zuber A (1993) Tracer experiments in fractured rocks: matrix diffusion and the validity of models. *Water Resour Res* 29:2723
- Manighetti I, King GCP, Gaudemer Y, Scholtz CH, Doubre C (2001) Slip accumulation and lateral propagation of active normal faults in Afar. *J Geophys Res* 106:13667–13696
- Mariner PE, Jin MQ, Studer JE, Pope GA (1999) The first vadose zone partitioning inter-well tracer test for nonaqueous phase liquid and water residual. *Environ Sci Technol* 33(16):2825–2828

- McCallum SD, Riestenberg DE, Cole DR, Freifeld BM, Trautz RC, Hovorka SD, Phelps TJ (2005) Monitoring geologically sequestered CO₂ during the Frio Brine pilot test using perfluorocarbon tracers. In: Proceedings, Fourth Annual Conference on Carbon Capture and Sequestration DOE/NETL
- Meier PM, Carrera J, Sánchez-Vila X (1998) An evaluation of Jacob's method for the interpretation of pumping tests in heterogeneous formations. *Water Resour Res* 34(5):1011–1025
- Micarelli DU, Moretti I, Jaubert M, Moulouel H (2006) Fracture analysis in the south-western Corinth rift (Greece) and implication on fault hydraulic behavior. *Tectonophysics* 426:31–59
- Myers M, Stalker L, Ross A, Dyt C, Ho K-B (2012) Method for the determination of residual carbon dioxide saturation using reactive ester tracers. *Appl Geochem* 27:2148–2156
- Nelson NT, Oostrom M, Wietsma TW, Brusseau ML (1999) Partitioning tracer method for the in situ measurement of DNAPL saturation: influence of heterogeneity and sampling method. *Environ Sci Technol* 33(22):4046–4053
- NETL (2013) Site screening, site selection, and initial characterization for storage of CO₂ in deep geologic formations, 2013 revised edition. DOE/NETL-2013/1605. National Energy Technology Laboratory, USA
- Neufeld JA, Hesse M, Riaz A, Hallworth M, Tchelepi H, Huppert HE (2010) Convective dissolution of carbon dioxide in saline aquifers. *Geophys Res Lett* 37:L22404
- Neuman SP, Witherspoon PA (1969) Applicability of current theories of flow in leaky aquifers. *Water Resour Res* 5(4):817–829
- Niemi A, Bensabat J, Shtivelman V, Edlmann K, Guze P, Luquot L, Hingerl F, Benson SM, Pezard PA, Rasmusson K, Liang T, Fagerlund F, Gendler M, Goldberg I, Tatomir A, Lange T, Sauter M, Freifeld B (2016). Heletz experimental site overview, characterization and data analysis for CO₂ injection and geological storage. *Int J Greenhouse Gas Control* 48:3–23
- NIST (2010) Reference fluid thermodynamic and transport properties database (REFPROP): version 9.1
- Nottebohm M, Licha T, Sauter M (2012) Tracer design for tracking thermal fronts in geothermal reservoirs. *Geothermics* 43:37–44
- Nur A (1971) Effects of stress on velocity anisotropy in rocks with cracks. *J Geophys Res* 76:2022–2034
- Oberdorfer P (2014) Heat transport phenomena in shallow geothermal boreholes-development of a numerical model and a novel extension for the thermal response test method by applying oscillating excitations. Ph. D. Thesis, University of Göttingen
- Oberdorfer P, Holzbecher E, Hu R, Ptak T, Sauter M (2013) A five spot well cluster for hydraulic and thermal tomography. In: Proceedings, 38th Workshop on Geothermal Reservoir Engineering, Stanford University, Stanford, CA, SGP-TR-198
- Paillet FL, White JE (1982) Acoustic modes of propagation in the borehole and their relationship to rock properties. *Geophys* 47:1215–1228
- Paterson L, Boreham C, Bunch M, Ennis-King J, Freifeld B, Haese R, Jenkins C, Raab M, Singh R, Stalker L (2013a) The CO₂CRC Otway stage 2B residual saturation and dissolution test: test concept, implementation and data collected. CO₂CRC report no: RPT11–3158
- Paterson L, Boreham C, Bunch M, Dance T, Ennis-King J, Freifeld B, Haese R, Jenkins C, LaForce T, Raab M, Singh R, Stalker L, Zhang Y (2013b) Overview of the CO₂CRC Otway residual saturation and dissolution test. *Energy Procedia* 37:6140–6148
- Paterson L, Boreham C, Bunch M, Dance T, Ennis-King J, Freifeld B, Haese R, Jenkins C, Raab M, Singh R, Stalker L (2014) CO₂CRC Otway Stage 2B residual saturation and dissolution test. In: Cook PJ (ed) Geologically storing carbon: learning from the Otway project experience. CSIRO Publishing, Melbourne, Australia, pp 343–380
- Pau G, Bell J, Pruess K, Almgren A, Lijewski M, Zhang K (2010) High-resolution simulation and characterization of density-driven flow in CO₂ storage in saline aquifers. *Adv Wat Resour* 33(4):443–455

- Place J, Sausse J, Marthelot J-M, Diraison M, Géraud Y, Naville C (2011) 3D mapping of permeable structures affecting a deep granite basement using isotropic 3C VSP data. *Geophys J Int* 186:245–263
- Plummer MA, Palmer CD, Mattson ED, Redden GD, Hull LC (2010) Advancing reactive tracer methods for monitoring thermal drawdown in enhanced geothermal reservoirs. Idaho National Laboratory, Preprint INL/CON-10-18881
- Poupon A, Loy M, Tixier M (1954) A contribution to electrical log interpretation in shaly sands. *J Petrol Technol* 6:27–34
- Prioul R, Donald A, Koupssell R, El Marzouki Z, Bratoon T (2007) Forward modeling of fracture-induced sonic anisotropy using a combination of borehole images and sonic logs. *Geophysics* 72:E135–E147
- Pruess K, Doughty C (2010) Thermal single-well injection-withdrawal tracer tests for determining fracture-matrix heat transfer area. In: *Proceedings, 35th workshop on geothermal reservoir engineering*, Stanford University, Stanford, CA, SGP-TR-188
- Ptak T, Piepenbrink M, Martac E (2004) Tracer tests for the investigation of heterogeneous porous media and stochastic modelling of flow and transport—a review of some recent developments. *J Hydrol* 294:122–163
- Qi R, LaForce TC, Blunt MJ (2009) Design of carbon dioxide storage in aquifers. *Int J Greenhouse Gas Control* 3:195–205
- Rao PSC, Annable MD, Kim H (2000) NAPL source zone characterization and remediation technology performance assessment: recent developments and applications of tracer techniques. *J Contam Hydrol* 45:63–78
- Rasmusson K, Rasmusson M, Fagerlund F, Bensabat J, Tsang Y, Niemi A (2014) Analysis of alternative push–pull-test-designs for determining in-situ residual trapping of carbon dioxide. *Int J Greenhouse Gas Control* 27:155–168
- Rasmusson K, Rasmusson M, Tsang Y, Niemi A (2016) A simulation study of the effect of trapping model, geological heterogeneity and injection strategies on CO₂ trapping. *Int J Greenhouse Gas Control* 52:52–72
- Read T, Bour O, Bense V, Le Borgne T, Goderniaux P, Klepikova MV, Hochreutener R, Lavenant N, Boschero V (2013) Characterizing ground water flow and heat transport in fractured rock using fiber-optic distributed temperature sensing. *Geophys Res Lett* 40:1–5
- Reimus P, Williams M, Vermeul V, Rose P, Leecaster K, Ayling B, Sanjuan R, Ames M, Dean C, Benoit D (2012) Use of tracers to interrogate surface area in single-well tracer tests in EGS Systems. In: *Proceedings, 37th Workshop on Geothermal Reservoir Engineering*, Stanford University, SGP-TR-194
- Renard P, Glenz D, Mejias M (2009) Understanding diagnostic plots for well-test interpretation. *Hydrogeol J* 17(3):589–600
- Riaz A, Hesse M, Tchelepi HA, Orr FM Jr (2006) Onset of convection in a gravitationally unstable diffusive boundary layer in porous media. *J Fluid Mech* 548:87–111
- Rodrigues JD (1983) The Noordbergum effect and characterization of aquitards at the Rio Maior Mining Project. *Ground Water* 21(2):200–207
- Rutqvist J (2012) The geomechanics of CO₂ storage in deep sedimentary formations. *Geotech Geol Eng* 30:525–551
- Sánchez-Vila X, Girardi JP, Carrera J (1995) A synthesis of approaches to upscaling of hydraulic conductivities. *Water Resour Res* 31(4):867–882
- Sánchez-Vila X, Carrera J, Girardi JP (1996) Scale effects in transmissivity. *J Hydrol* 183(1):1–22
- Saripalli KP, Kim H, Rao PSC, Annable MD (1997) Measurement of specific fluid–fluid interfacial areas of immiscible fluids in porous media. *Environ Sci Technol* 31:932–936
- Saripalli KP, Rao PSC, Annable MD (1998) Determination of specific NAPL–water interfacial areas of residual NAPLs in porous media using the interfacial tracers technique. *J Contam Hydrol* 30:375–391
- Schaffer M (2013) On the possibility of using organic molecules in the characterization of subsurface processes (PhD Thesis). University of Goettingen, Germany

- Schaffer M, Maier F, Licha T, Sauter M (2013) A new generation of tracers for the characterization of interfacial areas during supercritical carbon dioxide injections into deep saline aquifers: kinetic interface-sensitive tracers (KIS tracer). *Int J Greenhouse Gas Control* 14:200–208
- Schaffer M, Niedbala A, Maier F, Idzik KR, Wilke M, Licha T (2015) Recent progress on hydrolyzable compounds as thermo-sensitive tracers for investigating the thermal drawdown of geothermal reservoirs. In: *Proceedings, 40th workshop on geothermal reservoir engineering*, Stanford University, Stanford, CA, SGP-TR-204
- Schlumberger (1991) *Log interpretation principles/applications*. Schlumberger education services, Texas
- Schmittbuhl J, Schmitt F, Scholtz CH (1995) Scaling invariance of crack surfaces. *J Geophys Res* 100:5953–5973
- Semprini L, Hopkins OS, Tasker BR (2000) Laboratory, field and modeling studies of radon-222 as a natural tracer for monitoring NAPL contamination. *Transp Porous Media* 38:223–240
- Sharma AN, Luo D, Walter MT (2012) Hydrological tracers using nanobiotechnology: proof of concept. *Environ Sci Technol* 46:8928–8936
- Shook GM, Forsmann JH (2005) *Tracer interpretation using temporal moments on a spreadsheet*. Idaho National Laboratory
- Shook GM, Ansley SL, Wylie A (2004) *Tracers and tracer testing: design, implementation, and interpretation methods*. INEEL/EXT-03-01466
- Sibson RH (1977) Fault rocks and fault mechanisms. *J Geol Soc Lond* 133:191–213
- Sone H, Zoback MD (2014) Viscous relaxation model for predicting least principal stress magnitudes in sedimentary rocks. *J Pet Sci Eng* 134:416–431
- Sulem J (2007) Stress orientation evaluated from strain localization analysis in Aigion faults. *Tectonophysics* 442:3–13
- Sulem J, Vardoulakis I, Ouffroukh H, Boulon M, Hans J (2004) Experimental characterization of the thermos-poro-mechanical properties of the Aigion fault gouge. *CR Geosci* 336:455–466
- Surdam RC (ed) (2013) *Geological CO₂ storage characterization—the key to deploying clean fossil energy technology*. Springer, New York
- Tang JS (2005) Extended Brigham model for residual oil saturation measurement by partitioning tracer tests. *Soc Pet Eng SPE paper* 84874
- Tatomir AB, Schaffer M, Kissinger A, Hommel J, Nuske P, Licha T, Helmig R, Sauter M (2015) Novel approach for modeling kinetic with respect to time-dependent interfacial area change for the optimization of supercritical carbon dioxide injection into deep saline aquifers. *Int J Greenhouse Gas Control* 33:145–153
- Theis CV (1935) The relation between the lowering of the piezometric surface and the rate and duration of discharge of a well using ground water storage. US Department of the Interior, Geological Survey, Water Resources Division, Ground Water Branch
- Tian L, Yang Z, Fagerlund F, Niemi A (2016) Effects of permeability heterogeneity on CO₂ injectivity and storage efficiency coefficient. *Greenhouse Gas Sci Technol* 6:112–124
- Tomich JF, Dalton RL Jr, Deans HA, Shallenberger LK (1973) Single-well tracer method to measure residual oil saturation. *J Petrol Technol* 25(2):211–218
- Tong F, Niemi A, Yang Z, Fagerlund F, Licha T, Sauter M (2013) A numerical model of tracer transport in a non-isothermal two-phase flow system for CO₂ geological storage characterization. *Transp Porous Media* 98:173–192
- Urosevic M, Pevzner R, Kopic A, Wisman P, Shulakova V, Sharma S (2010) Time-lapse seismic monitoring of injection into a depleted gas reservoir—Naylor Field, Australia. *Lead Edge* 29:164–169
- Vandenbohede A, Louwyck A, Lebbe L (2009) Conservative solute versus heat transport in porous media during push–pull tests. *Transp Porous Media* 76:265–287
- Vandeweyer V, van der Meer B, Hofstee C, Mulders F, D’Hoore D, Graven H (2011) Monitoring the CO₂ injection site: K12-B. *Energy Procedia* 4:5471–5478
- Verdon JP, Kendall J-M, White DJ, Angus DA (2011) Linking microseismic event observations with geomechanical models to minimise the risks of storing CO₂ in geological formations. *Earth Planet Sci Lett* 305:143–152

- Verruijt A (1969) Elastic storage of aquifers. In: de Wiest RJM (ed) Flow through porous media. Academic Press, New York, pp 331–376
- Vilarrasa V, Bolster D, Olivella S, Carrera J (2010) Coupled hydromechanical modeling of CO₂ sequestration in deep saline aquifers. *Int J Greenhouse Gas Control* 4:910–919
- Vilarrasa V, Carrera J, Olivella S (2013) Hydromechanical characterization of CO₂ injection sites. *Int J Greenhouse Gas Control* 19:665–677
- Vulava VM, Perry EB, Romanek CS, Seaman JC (2002) Dissolved gases as partitioning tracers for determination of hydrogeological parameters. *Environ Sci Technol* 36:254–262
- Willmann M, Carrera J, Sánchez-Vila X, Vázquez-Suñé E (2007) On the meaning of transmissivity values obtained from. *Hydrogeol J* 15(5):833–842
- Winkler KW, Liu HL, Johnson DL (1989) Permeability and borehole Stoneley waves: comparison between experiment and theory. *Geophys* 54:66–75
- Wuerdemann H, Moeller F, Kuehn M, Heidug W, Christensen NP, Borm G, Schilling FR, the CO₂SINK Group (2010) CO₂SINK—from site characterisation and risk assessment to monitoring and verification: one year of operational experience with the field laboratory for CO₂ storage at Ketzin, Germany. *Int J Greenhouse Gas Control* 4(6) 938–951
- Xu T, Apps JA, Pruess K (2005) Mineral sequestration of carbon dioxide in a sandstone–shale system. *Chem Geol* 217:295–318
- Yeh T-CJ, Liu S (2000) Hydraulic tomography: development of a new aquifer test method. *Water Resour Res* 36(8):2095–2105
- Yilmaz Ö (2001) Seismic data analysis, society of exploration geophysicists
- Zatsepin SV, Crampin S (1997) Modelling the compliance of crustal rock-I. Response of shear-wave splitting to differential stress. *Geophys J Int* 129:477–494
- Zhang LQ, Yue ZQ, Yang ZF, Qi JX, Liu FC (2006) A displacement-based back-analysis method for rock mass modulus and horizontal in situ stress in tunnelling—illustrated with a case study. *Tunn Undergr Space Technol* 21:636–649
- Zhang Y, Freifeld B, Finsterle S, Leahy M, Ennis-King J, Paterson L, Dance T (2011) Single-well experimental design for studying residual trapping of supercritical carbon dioxide. *Int J Greenhouse Gas Control* 5:88–98
- Zoback MD, Barton CA, Brudy M, Castillo DA, Finkheiner T, Grollimund BR, Moos DB, Peska P, Ward CD, Wiprut DJ (2003) Determination of stress orientation and magnitude in deep wells. *Int J Rock Mech Min Sci* 40:1049–1076
- Zuber A, Motyka J (1994) Matrix porosity as the most important parameter of fissured rocks for solute transport at large scales. *J Hydrol* 158:19–46